+

Final Scientific/Technical Report

Federal Agency and Organization: DOE EERE – Geothermal Technologies Program

Recipient Organization: University of Utah
DUNS Number: 009095365
Recipient Address: 423 Wakara Way, suite 300, Salt Lake City, UT 84108

Award Number: DE-EE0005521

Project Title: Innovative computational tools for reducing exploration risk through integration of water-rock interactions and magnetotelluric surveys

Project Period: September 30, 2011 to June 30, 2014

Principal Investigator: Dr. Joseph Moore
Research Professor
jmoore@egi.utah.edu
801-585-6931

Date of Report Submission: April 20, 2017

Reporting Period: Sept. 30, 2011 - Jun. 30, 2015

Report Frequency: Final

Project Partners: Cyrq Energy and Terra-Gen Operating Co, LLC.

DOE Project Team: DOE Contracting Officer – Laura Merrick
DOE Project Officer – Mark Ziegenbein
Project Monitor – Grant Logsdon

DE-EE0005521
Joseph Moore
FINAL REPORT

INNOVATIVE COMPUTATIONAL TOOLS FOR REDUCING EXPLORATION RISK THROUGH INTEGRATION OF WATER-ROCK INTERACTIONS AND MAGNETOTELLURIC SURVEYS

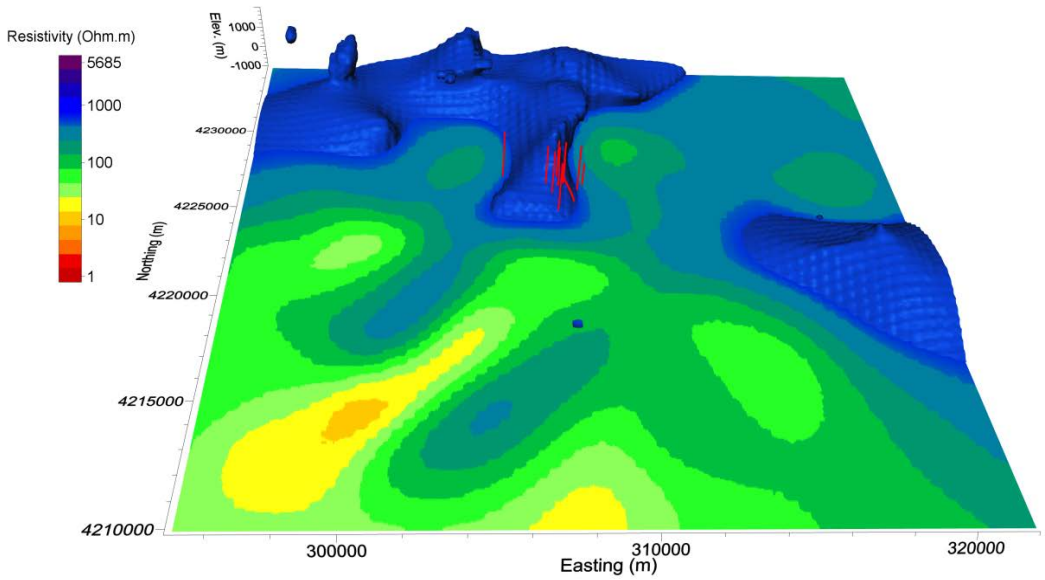

Submitted by Energy & Geoscience Institute at the University of Utah

April 2017

EXECUTIVE SUMMARY

Mapping permeability distributions in geothermal reservoirs is essential for reducing the cost of geothermal development. To avoid the cost and sampling bias of measuring permeability directly through drilling, we require remote methods of imaging permeability such as geophysics. Electrical resistivity (or its inverse, conductivity) is one of the most sensitive geophysical properties known to reflect long range fluid interconnection and thus the likelihood of permeability. Perhaps the most widely applied geophysical methods for imaging subsurface resistivity is magnetotellurics (MT) due to its relatively great penetration depths. A primary goal of this project is to confirm through ground truthing at existing geothermal systems that MT resistivity structure interpreted integratively is capable of revealing permeable fluid pathways into geothermal systems.

Phase 1 of this study adopts a two-step process for examining reservoir permeabilities using geochemical and geophysical perspectives. In step one, geochemical investigations focus on whole rock, oxygen isotope compositions of well cuttings to assess the extent of water/rock interactions. This is to determine if calculated water rock ratios (WRR) from chips can serve as a proxy for permeability in the absence of direct permeability measurements downhole. If so, this considerably enlarges the ground truth data base for testing whether resistivity is a reliable indicator of geothermal permeability.

In the second step, MT geophysical investigations have concentrated on the electrical resistivities of the reservoir rocks and the comparison of the resistivity structure to geochemically derived permeability and well productivity. We have utilized new procedures and algorithms for interpreting resistivity distributions from magnetotelluric (MT) data. The results have been integrated with new and existing geoscientific and drilling data to map permeability at the wellbore and field scale. Although MT surveys are widely used in the exploration of high-temperature resources, few studies have attempted to identify major structures beneath the shallow clay cap. Moreover in Phase I, the application of magnetotelluric data was expanded to include low- to moderate-temperature geothermal systems. The effects of improving drilling success rates on the Levelized Cost of Electricity (LCOE) were evaluated and show that even minor improvements in the confirmation success rate have a significant effect on the LCOE.

Four well characterized geothermal systems, all of which have been explored by deep drilling and production testing were investigated. Thermo Hot Springs (UT), Lightning Dock (NM) and Raft River (ID) are moderate temperature geothermal fields. Thermo Hot Springs and Lightning Dock are developed in Mesozoic and Paleozoic carbonate rocks. The reservoir at Raft River is hosted in Precambrian quartzite and quartz monzonite. Investigations at this field build on the DOE-funded EGS project “Concept testing and development at the Raft River geothermal field, Idaho”. The fourth system, Coso Hot Springs (CA), is a high-temperature resource developed in Mesozoic intrusive rocks ranging from diorite to granite in composition.

The following are the major results and implications of Phase I:

1. We have demonstrated that whole-rock oxygen isotope data and the calculated water/rock ratios are a useful guide to reservoir permeability at both the wellbore and field scale.

Oxygen isotope depletions and high water/rock ratios are strongly correlated with production intervals at Coso Hot Springs and Thermo Hot Springs. Low water-rock ratios characterize non-productive wells at Lightning Dock.

2. Using new three-dimensional (3D) MT inversion procedures and algorithms developed at EGI under DOE/GTP support, we have demonstrated that low resistivities can be used to map permeable pathways at Coso Hot Springs, Thermo Hot Springs, Raft River, and perhaps Lightning Dock.

3. Integration of MT surveys with temperature, mineralogic and isotopic data from low-cost slim holes may represent the most cost effective approach to evaluating unexplored or buried geothermal systems. Near-wellbore permeabilities derived from rock isotopic compositions together with mineral and fluid chemistry investigations can constrain the significance of the MT structure, which in turn can extrapolate permeability and identify fluid sources at broader reservoir scales.

4. All of the criteria required for positive decision to move to Phase II have been met.

INTRODUCTION AND TECHNICAL APPROACH

Water-rock interactions play a critical role in defining the physical and geochemical properties of geothermal reservoir and the overlying caprocks. With decreasing temperature, from the base of a geothermal system to the surface, the rocks undergo a series of mineralogic and physical changes that include the formation of propylitic (epidote-bearing), phyllic (illite-bearing), and argillic (clay-bearing) mineral assemblages. These mineralogic changes are accompanied by changes in the rocks densities and electrical conductivities. The electrical geophysical exploration methods, and in particular MT surveys, are routinely utilized by the geothermal industry to locate and characterize geothermal systems. The primary objective of these surveys has been to define the argillically altered, electrically conductive clay caps that form above the reservoir.

Within high temperature systems, the minerals that form in the underlying reservoir, e.g. illite, epidote and other silicate phases, are electrically resistive, and consequently rock conductivities decrease. Although inferences can be made regarding the general locations of the upflow zones and those portions of the reservoir where temperatures exceed about 220°C, the upper limit of smectite-bearing clays, it has not been possible to accurately characterize reservoir permeabilities and temperature distributions. This problem of characterizing permeability distributions in low- to moderate-temperature geothermal systems where reservoir temperatures do not significantly exceed 220°C is much more difficult because the electrical contrast between the reservoir and caprock may be significantly reduced. These moderate temperature reservoirs are found throughout the Basin and Range and in many parts of the Imperial Valley. In addition, these geothermal systems are potential targets for development of EGS and deep sedimentary reservoirs.

The study is divided into two phases. The primary objective of Phase 1 is to establish the interrelationships between reservoir permeabilities, the extent of water-rock interaction and reservoir resistivities. The research takes advantage of high quality, recently deployed MT surveys and the 3D algorithms that have recently been advanced by the Energy & Geoscience Institute (EGI) for the interpretation of MT data by Wannamaker and others.

The original proposal considered the investigation of at least two geothermal systems in Phase 1. However, the 2013 Peer Review Panel concluded the existing data set was insufficient to characterize the relationship between permeability, resistivity and alteration. With the concurrence of the DOE Project Manager, work was initiated on two additional geothermal systems using the existing funding. The four systems include Coso Hot Springs (CA), Thermo Hot Springs (UT), Lightning Dock (NM) and Raft River (ID). These geothermal systems were chosen because recently conducted MT surveys, cuttings, and geophysical logs from deep drill holes were available. The reservoirs at Thermo Hot Springs, Lightning Dock and Raft River host moderate temperature geothermal fluids. Thermo Hot Springs and Lightning Dock are developed in Mesozoic and Paleozoic carbonate rocks. The reservoir at Raft River is developed in Precambrian quartzite and quartz monzonite. Investigations at this field build on the DOE-funded EGS project “Concept testing and development at the Raft River geothermal field, Idaho”. The fourth system, Coso Hot Springs (CA), is a high-temperature resource developed in Mesozoic intrusive rocks ranging from diorite to granite in composition.

The validity of using isotope data to map water-rock interactions in hydrothermal ore deposits has been well established (refer to Task 1.3). However, the application of isotopic data to mapping reservoir permeability in geothermal systems has not been demonstrated. Similarly, the scientific basis for utilizing MT as a geothermal exploration tool has been clearly demonstrated (Cumming and Mackie, 2010). It is now well understood that the reservoir mineralogy, water content (e.g. permeability), water composition and distribution, and temperature all influence reservoir resistivity. Various combinations of these factors can result in a non-unique solution and similar resistivities.

In order to develop the framework and procedures required to relate reservoir permeability to resistivity under Task 3, two hypotheses will be tested and verified at each site. These are:

1. Is there a relationship between reservoir permeability and the degree of oxygen isotopic depletion of the rock as expressed as water-rock ratios?

2. Is there a relationship between reservoir permeability, reservoir mineralogy and the resistivity of the reservoir determined from MT data?

PHASE I – PROOF OF CONCEPT – FEASIBILITY ASSESSMENT

The purpose of the proposed tasks under Phase I are to evaluate rock characteristics (and their variability) that can be related to permeability, temperature and electrical conductivity. Particular emphasis will be placed on the thermally sensitive smectite-bearing clay minerals and on permeabilities recorded by the oxygen isotopic compositions of the rocks. Comprehensive 3D MT models of the systems will be developed. The procedures required to relate reservoir permeabilities and temperatures to the electrical conductivities will be established for two of the well-documented sites. The results will be compared to any recently completed and available reservoir permeability models based on a rate-time analysis.

Task 1.0. Sample Collection and Analyses

Task 1.1. Collection of Rock Samples and Geothermal Data

Samples will be collected from the reservoir and caprock sections of selected existing wells from two systems for petrographic and isotopic analyses. The samples will be analyzed by X-ray diffractometry to determine the type, characteristics (e.g. percent smectite in the clay minerals) and the abundances of the clay minerals and other phases in the rocks. Both the whole rock and the clay fraction (<5 micrometer fraction) will be analyzed. Thin section petrography will be used to identify the rock types, sample mineralogy and mineral textures and paragenetic relationships. Maps of clay abundances and types will be prepared. A suite of core and cuttings samples representing important environments within the geothermal fields are available for study at EGI's Sample Library. Additional samples may be provided from industry partners. The locations of major fracture zones will be obtained from the well logs. Samples from different alteration zones and displaying different degrees of alteration will be collected for whole-rock ^{18}O isotopic analyses. As discussed in the following sections, the isotopic data will be used to assess water-rock ratios, a measure of the time-integrated permeability of the system.

Table 1.1.1 summarizes the types of data available for each of the four geothermal systems examined in this study.

Table 1.1.1. Summary of data provided by industry partners for the four fields studied.

	Geologic maps	Drill cuttings	Lithologic (mud) logs	T/P/S Logs	Water chemistry	Water isotopes	Whole-rock isotopes	Gravity	MT	Reflection seismic surveys	Microseismic surveys	Aeromagnetic surveys	Electrical surveys
Lightning Dock	✓	✓	✓	✓	✓	✓		✓	✓	✓		✓	✓
Thermo Hot Springs	✓	✓	✓	✓	✓			✓	✓				
Raft River	✓	✓	✓	✓	✓			✓	✓				
Coso Hot Springs	✓	✓	✓	✓	✓	✓	✓		✓				

Task 1.2. X-ray Diffraction and Petrographic Analyses

Whole-rock and clay X-ray diffraction (XRD) analyses will be conducted in the XRD laboratory at EGI. The < 5 micrometers portion of the sample will be analyzed to identify individual clay species and the extent of smectite interlayering. Clay abundances will be determined from the whole-rock scans.

Table 1.2.1 illustrates the number of X-ray diffraction (XRD) and petrographic (thin section) analyses performed on each of the four fields. X-ray diffraction results are presented in Appendix 1, Task 1.2.

Table 1.2.1. Number of samples analyzed from each field by well.

Field	Well	XRD	Thin section
Lightning Dock	45-07	30	30
	47-07	43	43
	53-07	62	62
	53-07 ST-1	25	25
	55-07	57	57
	63-07	50	50
	TG 52-07	16	16
Thermo	13-34A	70	70
	63-33	62	62
	17-34	69	69
	Nov-34	2	2
	24-34	1	1
	52-34	1	1
Raft River	RRG-1*	4	4
	RRG-2*	35	27
	RRG-3 ST*-1	19	19
	RRG-3A*	2	2
	RRG-3C*	9	7
	RRG-3D*	45	45
	RRG-7*	11	28
	RRG-9*	88	97
	RRG-9 ST-1*	23	23
Coso Hot Springs	33A-7*	25	25
	33A-7	36	36
	33A-7 ST-1*	25	25
	83-11*	34	34
	68-6	17	17
	73-19	17	17
	42A-16*	31	31
	51A-16*	25	25

	41-33*	15	5
	41A-33*	20	11
	41B-33*	15	6

(*Previously acquired data)

Task 1.3. Whole-rock Oxygen Isotope Analyses

An important challenge is to relate the petrologic and geochemical indicators of rock permeability more reliably to the electrical resistivity data. We propose a multi-disciplinary approach to establishing the connections between permeability and $^{18}O/^{16}O$ depletion, clay mineral abundance and textural indicators of permeability by employing a suite of techniques that include the following: oxygen isotope analyses of whole rock samples and vein minerals; integrated automated mineralogy and petrography; and Scanning Electron Microscopy.

The $\delta^{18}O$ value of vein minerals, coupled with temperature information (from direct reservoir measurements, fluid/mineral geothermometers, or fluid inclusions), will allow calculation of the $\delta^{18}O$ value of the fluid at various locations. When combined with the measured $^{18}O/^{16}O$ depletions in the host rocks, the W/R ratio—and permeability—can be assessed. The results will be compared with the reservoir permeability model, vein abundances, fracture density (where core is available) and mineral abundances in the same sample and with permeability data from well logs (e.g. lost circulation zones, drilling breaks) to evaluate permeability at different scales.

Table 1.3.1 illustrates the number of isotope analyses performed on samples from each of the four fields. The analytical results are presented in Appendix 1, Task 1.3.

Theoretical Basis for the Calculation of Water-Rock Ratios

The degree of fluid-rock interaction in terms of the water/rock mass ratio can be determined from relatively simple mass balance calculations. Assuming equilibration between the rock and water, the water/rock (W/R_c) ratio for a closed system can be calculated from the relationship:

$$W/R_c = (\delta^{18}O_r^f - \delta^{18}O_r^i)/(\delta^{18}O_w^i - \delta^{18}O_w^f) \quad (1)$$

where $\delta^{18}O_r^f$ is the measured $\delta^{18}O$ value of the exchanged rock in the geothermal system, $\delta^{18}O_r^i$ is the initial $\delta^{18}O$ value of the rock (generally assumed to be the highest measured $\delta^{18}O$ value), $\delta^{18}O_w^i$ is the initial oxygen isotopic composition of the water, generally assumed to be represented by the local meteoric water, and $\delta^{18}O_w^f$ is the $\delta^{18}O$ value of the reservoir fluid, determined from analyses of the produced waters. Alternatively, the W/R_o ratio can be calculated assuming an open-system, that is, a system in which the water is not recycled (one-pass). The W/R_o ratio for an open system is given by the relationship (Criss and Taylor, 1986):

$$W/R_o = \ln\{(W/R)_c + 1\} \quad (2)$$

Values of W/R ratio calculated with the open-system end member will be lower, for a given amount of $^{18}O/^{16}O$ depletion in the rock.

Figure 1.3.1a represents a water-dominated system where all the rock interacts with the water, but not all the water will interact with the rock; alternatively, Figure 1.3.1b represents a rock-dominated system where all the water present (confined to fractures and micropores) will interact with the rock, but only a small fraction of the rock will ever interact with the water. As a result, these competing scenarios will exhibit different oxygen isotopic exchange profiles (Fig. 1.3.2). Assuming equilibrium is obtained, the extent of $^{18}O/^{16}O$ depletion of the rock in a water-dominated system will be significant (line b, Fig. 1.3.2) while $^{18}O/^{16}O$ enrichment of the water will be minimal (line a, Fig. 1.3.2); for a rock-dominated system, the extent of the $^{18}O/^{16}O$ depletion to the rock will be minimal (line f, Fig. 1.3.2) while the $^{18}O/^{16}O$ enrichment to the water will be significant (line e, Fig. 1.3.2).

Table 1.3.1. Number of oxygen isotope analyses performed on each field by well.

Field	Well	O isotope analyses
Lightning Dock	45-07	
	47-07	23
	53-07	22
	53-07 ST-1	5
	55-07	9
	63-07	13
	TG 52-07	
Thermo	13-34A	28
	63-33	31
	17-34	
	Nov-34	
	24-34	
	52-34	
Raft River	RRG-1*	
	RRG-2*	
	RRG-3 ST*-1	
	RRG-3A*	
	RRG-3C*	
	RRG-3D*	
	RRG-7*	
	RRG-9*	
	RRG-9 ST-1*	
Coso Hot Springs	33A-7*	
	33A-7	66
	33A-7 ST-1*	
	83-11*	
	68-6	67
	73-19	34
	42A-16*	
	51A-16*	
	41-33*	
	41A-33*	
	41B-33*	

(*Previously acquired data)

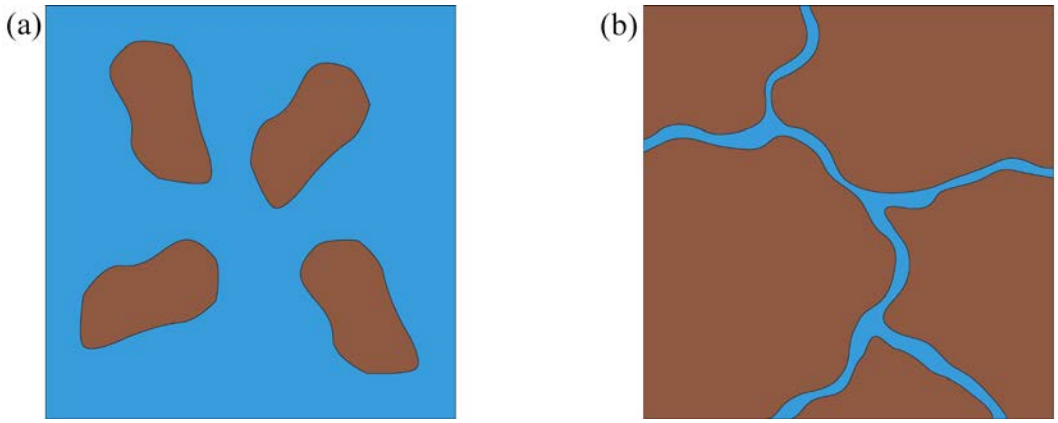

Fig. 1.3.1. Two model scenarios constructed to help illustrate the difference between a high W/R environment and a low W/R environment (b). In (a), all of the rock will interact with water while in (b), the fluid is only present in fractures and micropores and therefore, only a fraction of the rock will interact with water.

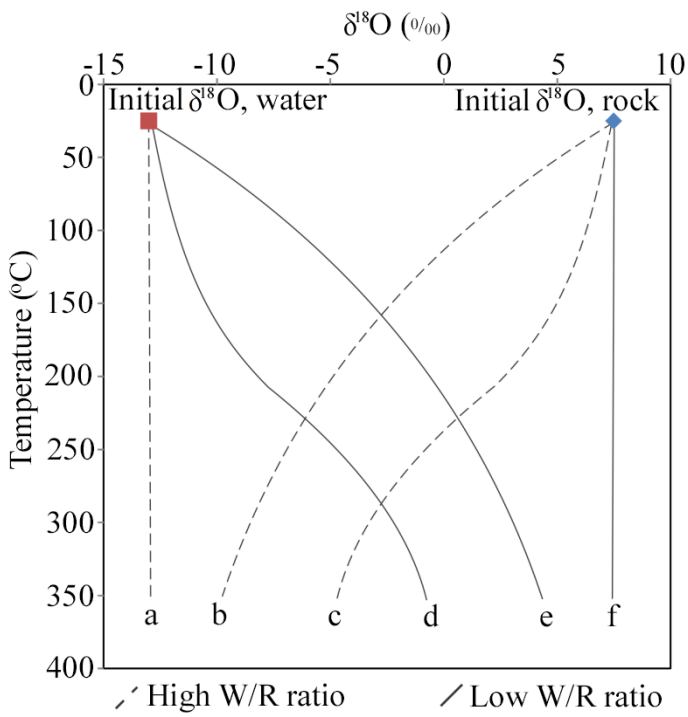

Fig. 1.3.2. A $\delta^{18}O$ vs. temperature plot constructed to display the evolution of the $\delta^{18}O$ values for rock and water as a result of kinetic and temperature variations. Dashed lines depict variations in high W/R environments while the solid lines depict variations in low W/R environments; lines "c" and "d" depict the evolution of systems unable to achieve equilibrium as a result of incomplete exchange while "b" and "e" relate to systems that have fully equilibrated.

The influences both temperature and kinetics have on the extent of the $^{18}O/^{16}O$ exchange between the fluid and rock is illustrated in Figure 1.3.2. Isotopic fractionation is a temperature dependent process (O'Neil, 1986); therefore, the extent of exchange required for these two components to obtain equilibrium will depend on the temperature at which exchange is occurring. In a water-dominated system (Fig. 1.3.1a), the final $\delta^{18}O$ value of the rock will become progressively lighter as temperature increases; however, in a rock-dominated system (Fig. 1.3.1b), the fluid will become progressively enriched with increasing temperature (the $\delta^{18}O$ value of rock will remain nearly constant for a rock-dominated system). When considering kinetic effects, the general exchange trends for both scenarios described above will still be observed, that is $\delta^{18}O$ rock values will decrease in a water-dominated system while $\delta^{18}O$ fluid values will increase in a rock-dominated system; however the extent of $^{18}O/^{16}O$ exchange will be limited (lines c & d of Fig. 1.3.2). Systems in which the fluid and rock are not able to obtain equilibrium will result in incomplete exchange and therefore the $\delta^{18}O$ values of the rock and water will deviate from the equilibrium values for a given temperature.

Task 2.0. Collection and Interpretation of Magnetotelluric Data

Using existing high-quality MT data, two well-characterized geothermal systems will be investigated: a geologically simple, high-temperature geothermal system and a geologically complex moderate-temperature system. For those sites that have been previously modeled, data from existing MT soundings will be combined with newly acquired MT soundings to develop a single resistivity model. Using our in-house 3D finite difference inversion program, we will determine if previously demonstrated relationships between reservoir permeabilities, degree and type of clay alteration, and temperature to the electrical resistivities can be documented in other parts of the field and in other geothermal systems. It is not yet known if the permeability structure of a moderate-temperature geothermal system can be defined using MT data; a further problem in low-to moderate-temperature environments is the common occurrence of nearby clay-bearing basins, which will also be imaged as conductive regions.

High quality MT data were acquired from all four geothermal systems. Since submission of the original proposal, the original finite difference algorithm we were using (modified from Uchida and Sasaki, 2006) was replaced by a new deformable finite element algorithm developed in-house under DOE/GTP support and described below. 3D inversions using our new capability were prepared for Coso Hot Springs, Lightning Dock, Thermo Hot Springs and Raft River. Descriptions of the MT inversions for the individual geothermal systems are included in Appendix 2.

MT plan maps and cross sections that illustrate the relationships between reservoir permeabilities and resistivity are discussed under Task 3.

Basis for Interpretation of MT Data

Magnetotellurics (MT) is a geophysical technique whereby naturally-occurring, broad-spectrum electromagnetic (EM) waves are used as source fields for imaging Earth's electrical conductivity structure (Vozoff, 1991, Simpson & Bahr, 2005; Chave and Jones, 2012). The method has been successfully used in geothermal systems to detect variations related to fluid flow and to map conductive alteration minerals (Wannamaker & Hohmann, 1991; Cumming and Mackie, 2007; Uchida and Sasaki, 2006; Spichak and Manzella, 2009; Wannamaker et al., 2007, 2013; Bertrand et al., 2012). The simulation and inversion of 3D diffusive EM responses for resistivity structure requires an algorithm that can handle a large range of structural scales due to possibly complex resistivity distributions and the wide frequency bandwidth of MT surveys (e.g., potentially seven or more orders of magnitude). Furthermore, in many geologic settings, the Earth's surface can show considerable topographic variation, which will have its own EM response and adds non-uniformity of receiver placement with respect to subsurface structure.

Inversion of MT data for this project was done using a new algorithm with unique capabilities by Kordy et al. (2015) at EGI/University of Utah. It uses a deformable finite element (FE) mesh and direct solvers to model the EM fields required to calculate MT responses and Frechet derivatives for a 3D resistivity distribution including topography. The program inverts all elements of the complex tensor impedance and the tipper. The resistivity distribution is determined using the data-space method as described by Siripunvaraporn et al. (2005), with an additional stabilizing functional promoting maximal spatial smoothness with respect to an a-priori structure. To minimize execution time, allow for larger data sets, and allow for a larger number of voxels in representing the resistivity structure, the program is designed to run efficiently on a multi-core workstation and make use of high-performance math libraries (PARDISO, PLASMA). Use of direct solvers for both the forward problem and the iterative parameter step is a particular strength of our algorithm; model convergence is rapid and monotonic, requiring typically ~10 iterations and achieving a fit comparable to data error.

The resistivity structure is represented using a FE mesh embedded in a 1D background. Generally, there are 10 z-layers of voxels above the ground surface (air). MT stations as modeled in the program may be laterally offset from their true location in order to accommodate the program requirement that the station be horizontally centered on a voxel. The FE mesh is deformed vertically to represent topography, using a digital elevation model down-loaded from the US Geological Survey website, http://gdex.cr.usgs.gov/gdex/. These background layer thicknesses represent the nominal voxel thicknesses before deforming them vertically to accommodate the surface topography. The starting model, also used as the a-priori constraint, was determined by 1D inversion of a sounding derived from the average of the off-diagonal impedances (a rotational invariant) over all frequencies, using the background layer thicknesses defined for the 3D inversion model.

Data quality was evaluated prior to the inversion; individual data found to be of poor quality were either assigned large errors to reduce their importance in determining the resistivity structure or flagged to be omitted. Error floors consist of 0.03 for the tipper data and for the impedance data (at a particular receiver and frequency) of the maximum of: the error assigned during data evaluation; 3.5%|data|; 3.5%|product of the principal impedances|$^{0.5}$. The misfit

(normalized root-mean-square error or nRMS) between predicted and observed data is measured as the norm of the data-weighted residual divided by the number of data squared.

Inversions were run on a 64-bit 24-cpu multi-core computer consisting of 4 Intel Xeon E5-4610 2.40GHz Hex-Core Processors, with 512GB RAM. This is an affordable, single-box hardware format exhibiting good scalability across the cores (Kordy et al., 2015).

Task 3.0. Develop the Framework and Procedures Required to Relate Reservoir Permeabilities to Electrical Resistivity Data

Reducing exploration risk through a better understanding of permeability and temperature distributions is dependent on better characterization of reservoir properties and their correlation with electrical resistivities and reservoir permeability models derived from dynamic data. The development of significantly improved procedures and models will enable better and quicker evaluation of economic prospects of hidden/new geothermal systems thereby reducing the cost of exploration.

We postulate that MT resistivity geophysical structure is a diagnostic indicator of geothermal fluid upflow. In this task, we test this hypothesis by comparing MT response inversion models to available permeability and oxygen isotope compositions for the four geothermal fields that were studied. Demonstration of these relationships is intended to result in improved geophysical and geochemical models that will form the framework for interpreting resistivity data.

The 3D MT inversions described in this task are based on new procedures and algorithms developed by Kordy, Wanamaker et al developed under DOE/GTP support. These procedures provide greater resolution of 3D resistivity structure than was available based upon previous algorithms.

Details of the mineral investigations are presented in Appendix 1. Low-resistivity smectite and/or interlayered illite-smectite or chlorite-smectite, which do not break down until temperatures exceed ~225ºC, are stable mineral phases throughout the explored depths of the moderate-temperature systems that were studied (Lightning Dock, Thermo, Raft River). On the other hand, Coso Hot Springs geothermal field is a high-temperature system in tight plutonic host rocks, and so the separation of fluid flow pathways from clay alteration effects in electrical resistivity should be more straightforward.

It must be recognized that the study is limited to four geothermal systems each with a finite quantity of available pertinent data to examine the geophysical and geochemical interrelationships. We believe the study has provided valuable insights into geophysical subsurface probing and interpretation, and underpins recommendations for Phase II progress.

Task 3.1. Coso Hot Springs

Coso Hot Springs provides an example of a high-temperature geothermal system (Fig. 3.1.1). The reservoir is developed in granitic to dioritic rocks with essentially nil porosity. Temperature distributions demonstrate that the fluids originate in the southern part of the field and then migrate upward and laterally to the north along a relatively narrow permeable fairway of fractured rocks (Fig. 3.1.2). Most of the 240 MWe originally produced at Coso came from this region of the field. There is currently no evidence of shallow dipping structures, changes in rock type, or extensively brecciated rock that could provide an explanation for the orientation of this fluid pathway.

Oxygen Isotope Data

Figures 3.1.2 shows the oxygen isotopic compositions of the rocks along a north-south (A-A') cross section. The cross section is based on 513 whole-rock oxygen isotope analyses, made available by Terra-Gen and 95 new whole-rock analyses obtained as part of this investigation. Wells 68-6, 33A-7 and 73-19 were studied in detail and the isotopic data from them is shown in Figure 3.1.3. Near surface values are consistent with those of the Central Sierra Nevada Batholith (Masi et al., 1981). The lowest isotopic values are found in the northern part of the reservoir, where the plume is shallowest. Nearby, active fumaroles are associated with a large area of advanced argillic alteration at Devil's Kitchen. This activity suggests high, near surface permeability.

In detail, the oxygen isotopic compositions of 33A-7, 68-6 and 73-19 appear to closely correlate with the locations of the production zones provided by Terra-Gen, with the greatest isotopic depletions (and highest water-rock ratios) occurring in rocks with the highest permeabilities. In 33-7A, depleted rocks extend several hundred meters above the production zone.

Analysis of the isotopic data

The measured difference in $\delta^{18}O$ value between the reservoir fluid and the most depleted whole-rock sample (measured Δ_{r-w}) in 33-A7 and 68-6 is considerably less than the equilibrium rock-water fractionation factor (equilibrium Δ_{r-w}) at the current measured temperature in these wells. The equilibrium Δ_{r-w} has been estimated assuming plagioclase ($X_{.An} = 0.4$) acts as a proxy for the rock (O'Neil and Taylor, 1967). The measured Δ_{r-w} in well 33A-7 at 2530 m is 4.18 ‰, whereas the equilibrium Δ_{r-w} for the measured temperature of 228ºC would be 7.13 ‰. In well 68-6, the measured Δ_{r-w} at 2941 m is 3.4 ‰, whereas the equilibrium Δ_{r-w} is 6.88 for the measured temperature of 234ºC. Thus the measured Δ_{r-w} values for these isotopically depleted zones in wells 33A-7 and 68-6 are smaller than the equilibration Δ_{r-w} values at current temperatures. These discrepancies are not the result of incomplete oxygen isotope exchange between the geothermal fluid and the rocks as incomplete isotopic exchange would produce measured Δ_{r-w} values greater than equilibrium Δ_{r-w} values; hence isotopic exchange kinetics is not the explanation for these differences.

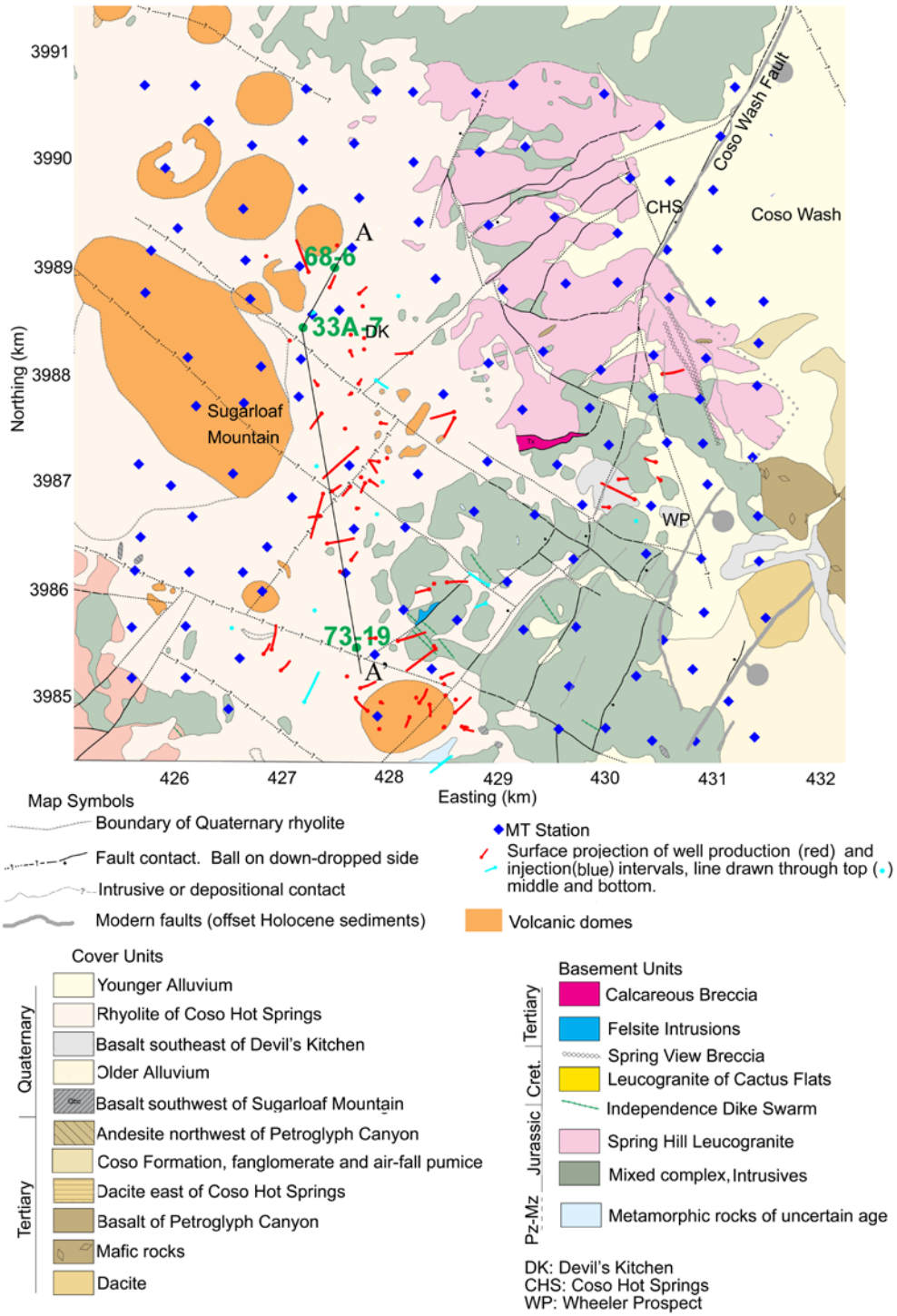

Fig. 3.1.1. Compilation map showing geologic structures, lithology, well production and injection intervals, with the MT stations used in inversion. Geological mapping extracted primarily from Whitmarsh (2002a, b); more recently compiled modern faults from Davatzes and Hickman (2006); well production and injection intervals provided by the U.S. Navy (F. Monastero, pers. comm.) courtesy of G. Newman and E. Gasperikova.

The discrepancies require either that the temperature of this fluid-rock isotopic exchange was higher than current temperatures, the $\delta^{18}O$ values of the geothermal fluids were lower, or a combination of both. Temperature would need to increase to 318° and 352°C in wells 33A-7 and 68-6, respectively, for the measured Δ_{r-w} values in these wells to correspond to equilibrium Δ_{r-w} values. Alternatively, the $\delta^{18}O$ values of the reservoir fluids in wells 33A-7 and 68-6 would have to decrease by 2.91 ‰ and 3.49 ‰, respectively. A decrease in the $\delta^{18}O$ value of the reservoir fluid implies an increase in the W/R ratio (and permeability) for the geothermal system as a whole. The implication of these data is that the rocks in 33A-7 and 68-6 were hotter and/or characterized by higher permeability in the past and that the current flow path is taking advantage of an earlier fracture zone.

The situation for well 73-19 is opposite that in wells 33A-7 and 68-6. Here, the Δ_{r-w} at 1411 m (depth of the most oxygen depleted whole rock sample is 8.03 ‰, whereas the equilibrium Δ_{r-w} for the measured temperature of 282°C would be 4.13 ‰. This discrepancy is interpreted to reflect incomplete isotopic exchange between rock and reservoir fluid, either from kinetic barriers to isotopic exchange or limited physical contact between reservoir fluid and rock owing to lower permeability, or both.

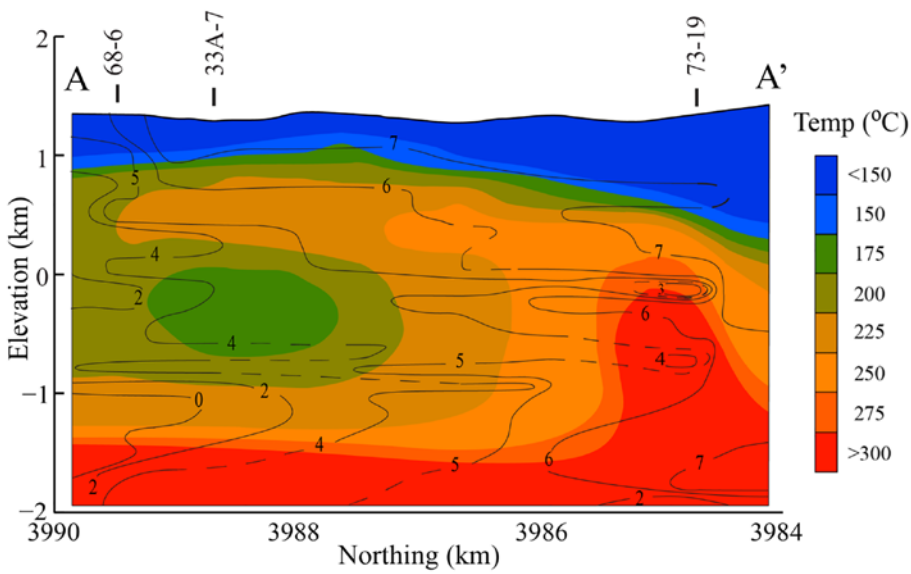

Fig. 3.1.2. Cross section showing the temperature and oxygen isotope distributions along a north–south transect (A-A'). Thermal waters originate in the southern part of the field where temperatures exceed 300°C and then migrate to the north along a narrow high permeability plume enclosed within the 225°C isotherm. Isotope data are shown and contoured in per mil. The main

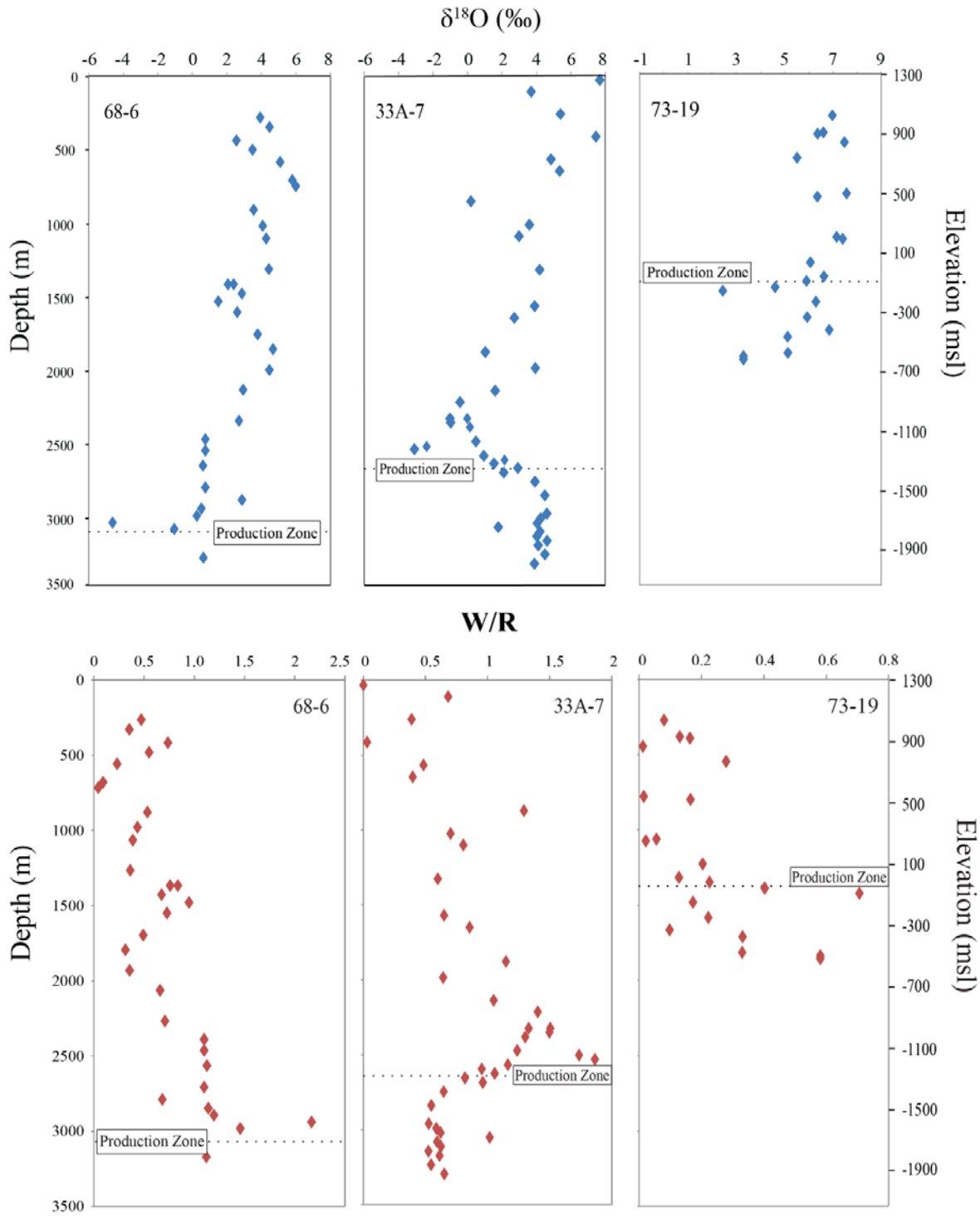

Fig. 3.1.3. Whole-rock oxygen isotope data for the three production wells studied. The most isotopically depleted rocks occur close to the major production zones. Calculated water-rock ratios are also shown on each figure.

MT Data

Data from 126 soundings in a swath covering the main producing area were selected for inversion. A compilation map showing geological structures and lithology, with the MT stations included, is provided in Figure 3.1.1. These MT data are part of a larger dataset of 210 sites, collected in three phases between 2004 and 2011. Data quality was evaluated prior to the inversion.

Figure 3.1.4 presents a series of plan maps at progressively greater depths. At the shallowest depth, numerous localized areas of low resistivity are present. At intermediate depths, the low resistivities are limited to two narrow well defined north-trending zones. The western plume is coincident with the west flank reservoir; the eastern plume coincides with the east flank reservoir. The two reservoirs appear to connect toward greater depths in the southeast portion of the field. In the deepest section, only the connection between the two reservoirs is apparent.

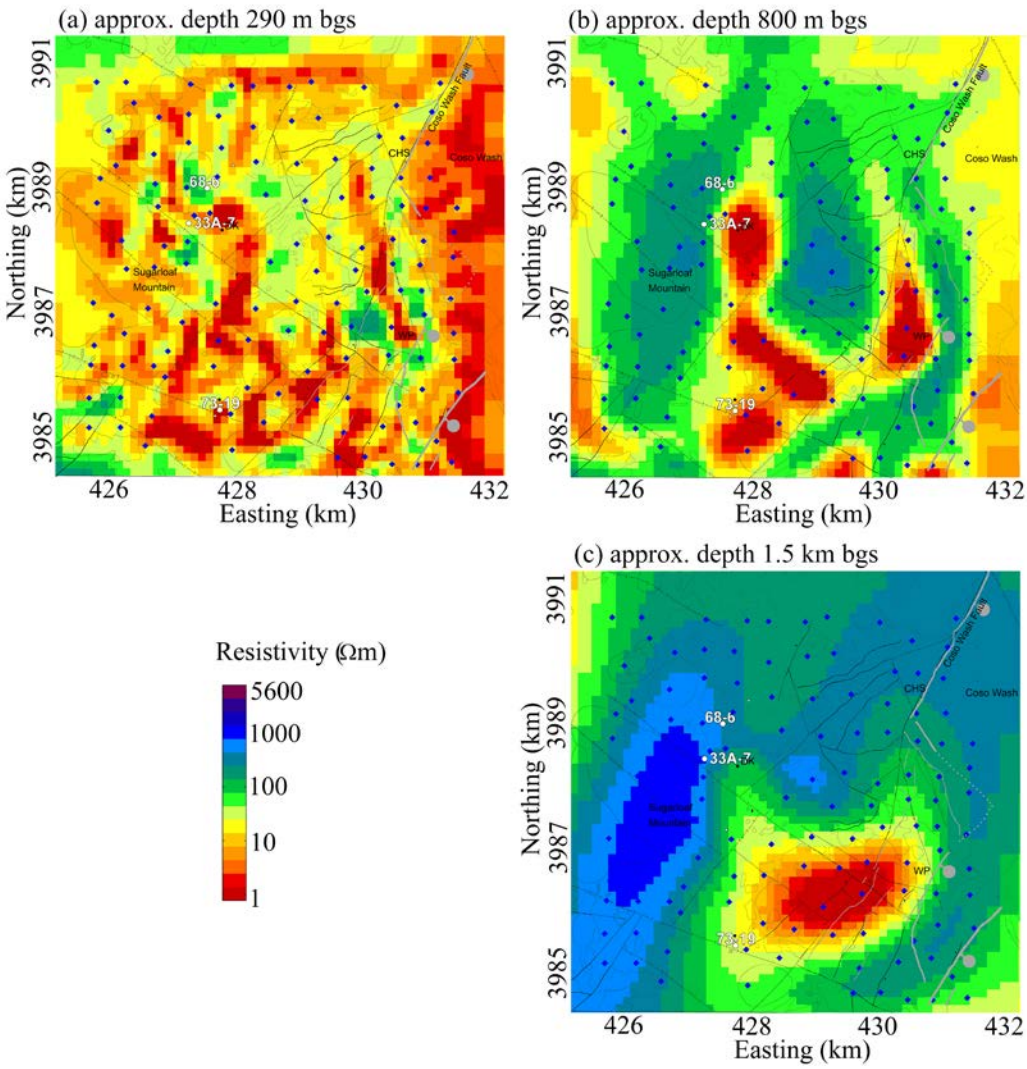

Fig. 3.1.4. Plan maps at approximate depths (bgs) of (a) 290 m; (b) 800 m; and (c) 1.5 km.

A north-south resistivity section along the strike of the west flank reservoir is shown in Figure 3.1.5. Low resistivities are found from the surface to the approximate base of smectite mineralization and conductive thermal gradients that corresponds approximately to the 150ºC isotherm. This zone, with resistivities less than about 5 ohm m is interpreted to represent the clay cap of the system. The X-ray diffraction data indicate the smectite content is only about 2%. The steep temperature gradients through the low-resistivity smectite zone are consistent with well data indicating that the near-surface permeabilities are low and that the resistivities are controlled by clay mineralization.

The low-resistivities at intermediate depths occur within the central portion of the west flank reservoir. At the southern end of the reservoir, the temperatures and moderately low resistivities define a pipe-like feature interpreted to represent a region of fluid upwelling. Temperatures within the region of lower resistivities are too high to reflect the formation of smectite. Thus, these low resistivities must be related to enhanced permeabilities and fluid flow. Elsewhere at Coso Hot Springs and below elevations of -1 to -2 km asl generally, the rocks become increasingly resistive reflecting their lower permeabilities and decreased fluid content.

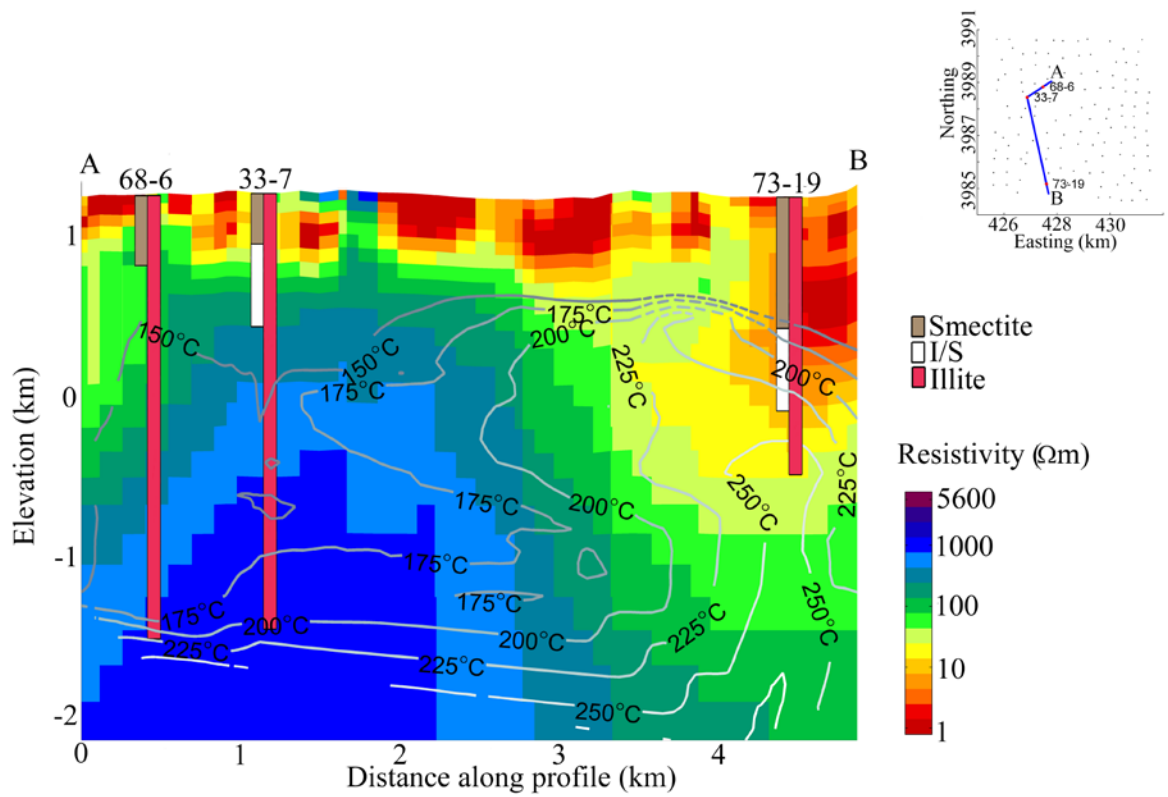

Fig. 3.1.5. Cross section through the wells, showing resistivities, clay mineralogy and temperature.

3.2. Lightning Dock

The Lightning Dock geothermal system, located in southern New Mexico is an example of a moderate temperature geothermal system. This is a blind geothermal system that was discovered in 1948 when a cotton farmer drilled a hot shallow water well (R. Bowers, pers. comm., 2015). The reservoir is developed in Mesozoic limestone and dolomite that underlies Tertiary volcaniclastic rocks. Locally, Tertiary silicic dikes intrude the sedimentary rocks. Five production tests greater than 1000 m depth have been drilled; the deepest reaching a depth of 2134 m and a temperature of 162ºC (Fig. 3.2.1). At this temperature, smectite is the stable clay phase.

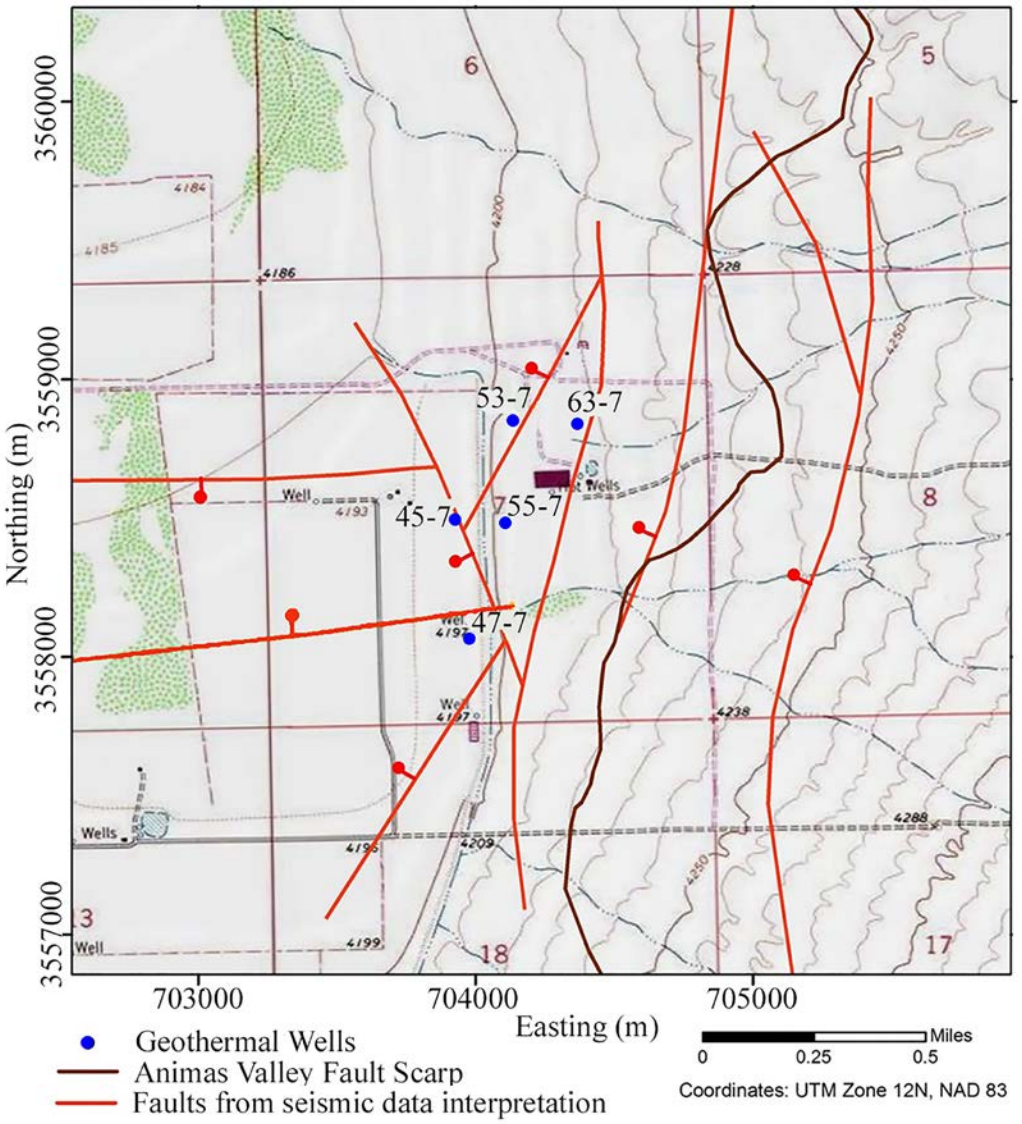

Fig. 3.2.1. Location of major structures and deep wells. Wells 53-7, 63-7, 55-7 and 47-7 were drilled into a horst block. 45-7 lies at the western edge of the block.

Although a hot shallow aquifer (<100 m) is present throughout the area, only one of the 5 recently drilled deep wells, 45-7, encountered commercial quantities of geothermal water. This well intersected a major fracture zone below about 700 m. No significant lost circulation or commercial flow rates were encountered in the other wells. The deep permeability structure of the field is not yet well understood but at this point appears tightly confined.

Oxygen Isotope Data

Whole-rock oxygen isotopic analyses were performed on 59 samples of carbonate rocks from 47-07, 53-07, 53-07ST, 55-07 and 63-07 at the University of Utah's SIRFER laboratory. Figure 3.2.2 shows the isotopic values obtained for the five wells.

The data display a narrow range of $\delta^{18}O$ values with little variation between or within wells. The average highest measured $\delta^{18}O$ value of +27 ‰) is nearly identical to the $\delta^{18}O$ value for a pristine marine carbonate rock (+23 ‰ to +26 ‰; Rao, 1990). Overall, these isotopic values and lack of significant isotopic depletions are consistent with the low permeabilities of the wells. Unfortunately, no isotopic data was collected from 45-07 because no cuttings were returned from the reservoir. Thus we do not know what the actual isotopic depletion and implied water-rock ratios may be for the Lightning Dock producing zone.

MT Data

Data from 60 MT soundings were provided by Cyrq Energy for this project. The locations of the survey sites are shown in (Fig. 3.2.3).

Discontinuities in the resistivities shown in the deeper plan maps and cross section are consistent with the presence of structures trending north-south along the western margin of the horst, northeast-southwest on the northern edge of the horst and northwest-south east along the eastern edge of the horst. The productive fault on the western margin of the horst was encountered in 45-7. The horst bounding fault locations are imaged in the cross section drawn through this commercial well.

Production well 45-7 lies within an isolated area of low resistivity that is imaged in the plan map shown for a depth of 1.06 km. In the cross section, the transition from low to high resistivity is nearly vertical, consistent with a steeply dipping fault. In contrast, the transitions from low to high resistivity on the basin margins dip at relatively shallow angles. Below an elevation of -1 km, resistivities increase to greater than 100 ohm.m, suggesting decreased permeabilities and/or more diffuse upward flow of the geothermal fluids.

Although not as definitive as the Coso Hot Springs geothermal field study, the results from Lightning Dock are consistent with our hypothesis at the outset of the Task 3 description. Unproductive wells are not associated with an oxygen isotope depletion trend. There is a conductor centered in plan view on the productive well, although it is weak and the association

perhaps non-unique. This is not entirely unexpected in a low-temperature, low-output geothermal field.

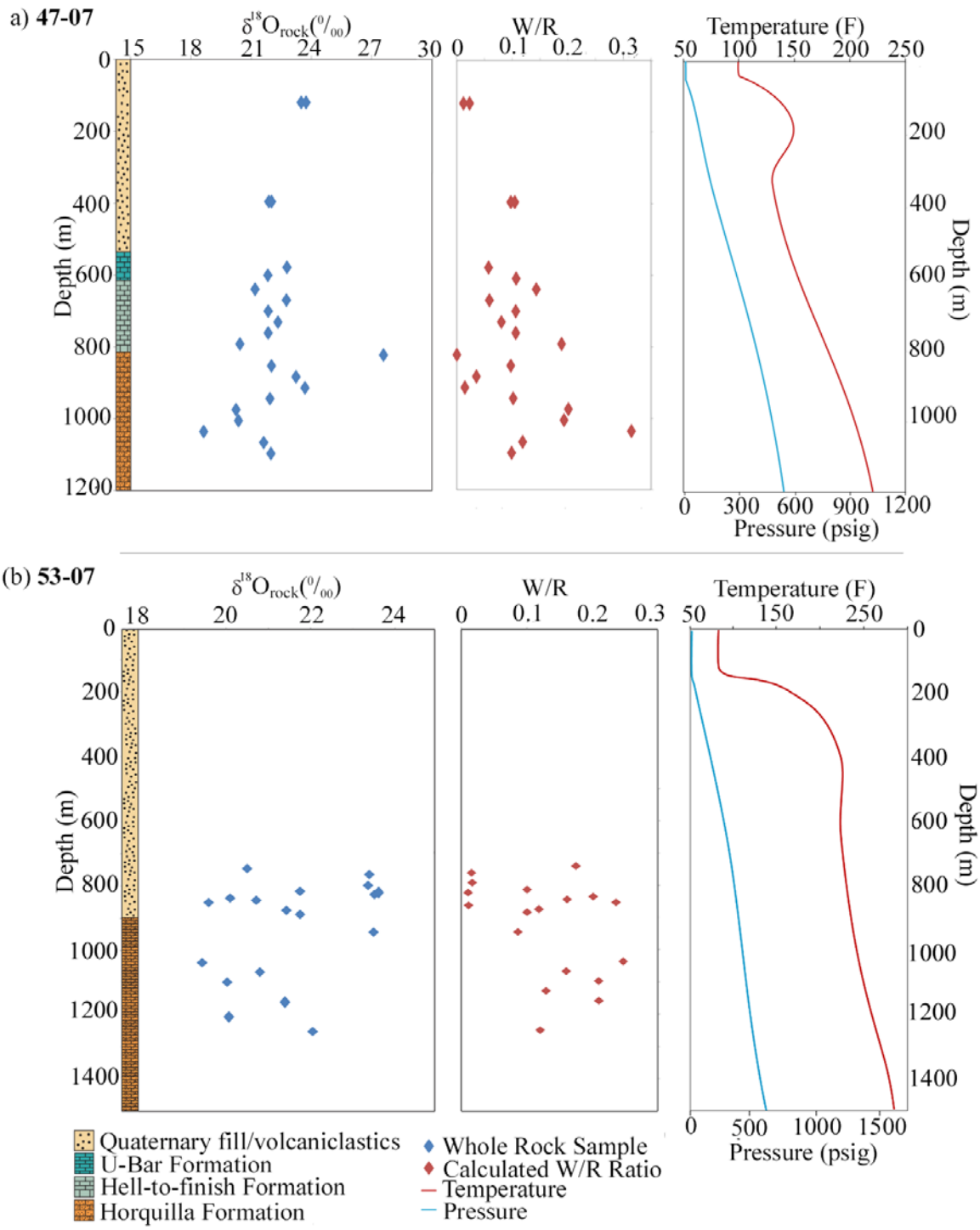

Figure 3.2.2. Measured $\delta^{18}O$ values, water-rock ratios and temperatures vs. depth for unproductive wells (a) 47-07, (b) 53-07, (c) 53-07ST1, (d) 55-07 and (e) 63-07.

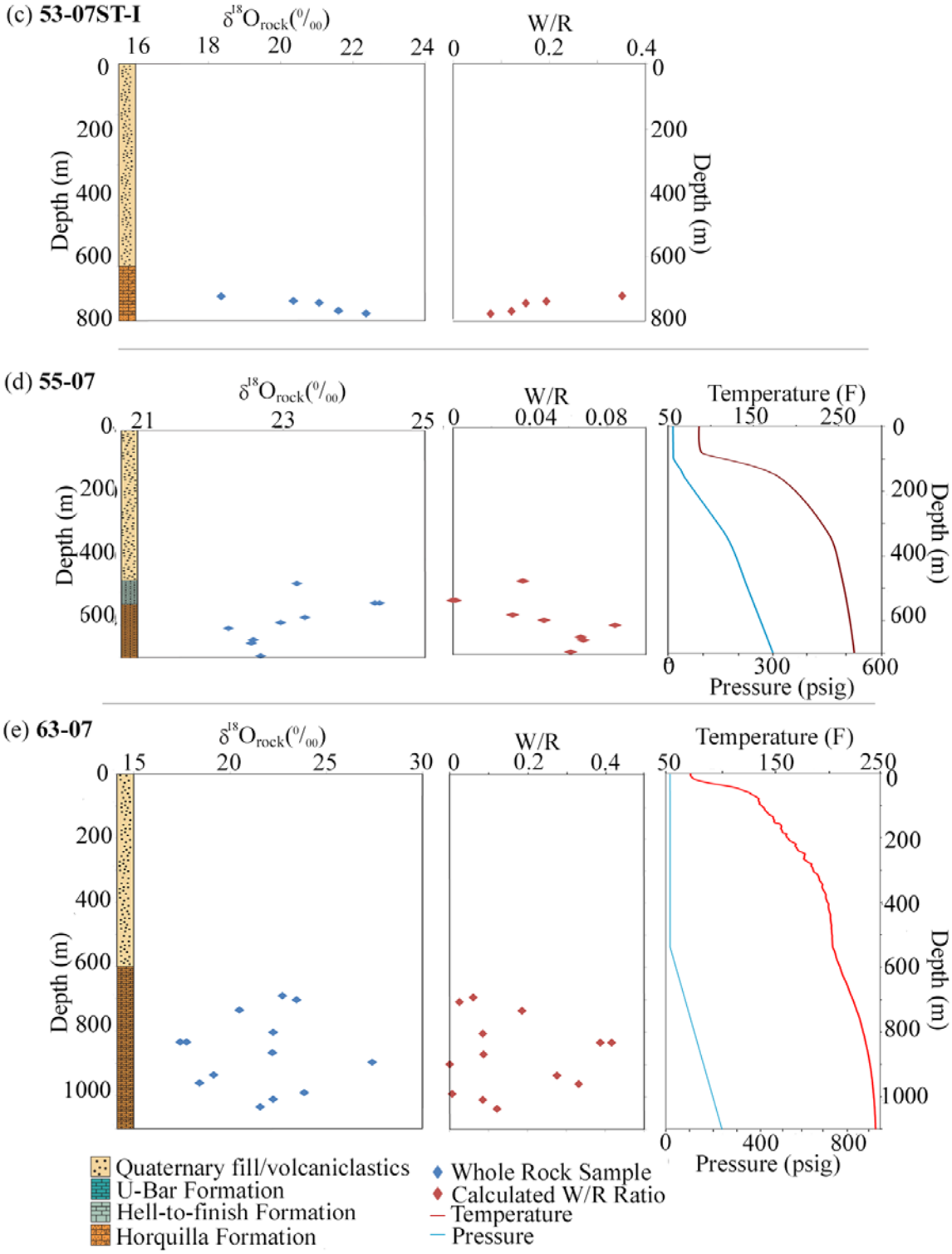

Fig. 3.2.2, continued.

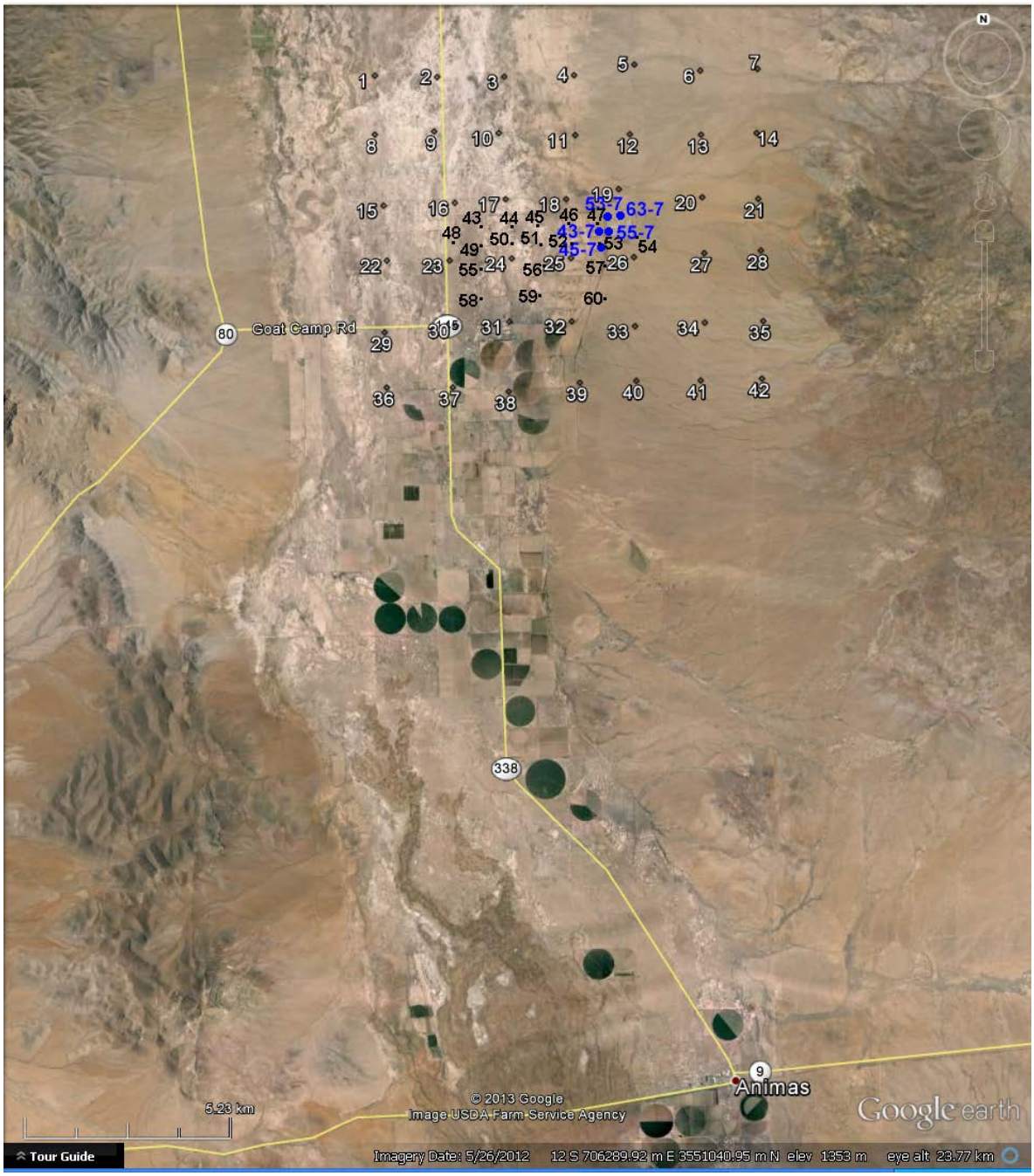

Fig. 3.2.3. Map of the survey area showing the MT station locations and the deep geothermal wells (blue). Data were collected in 2010 (white labels) and 2014 (black labels).

.

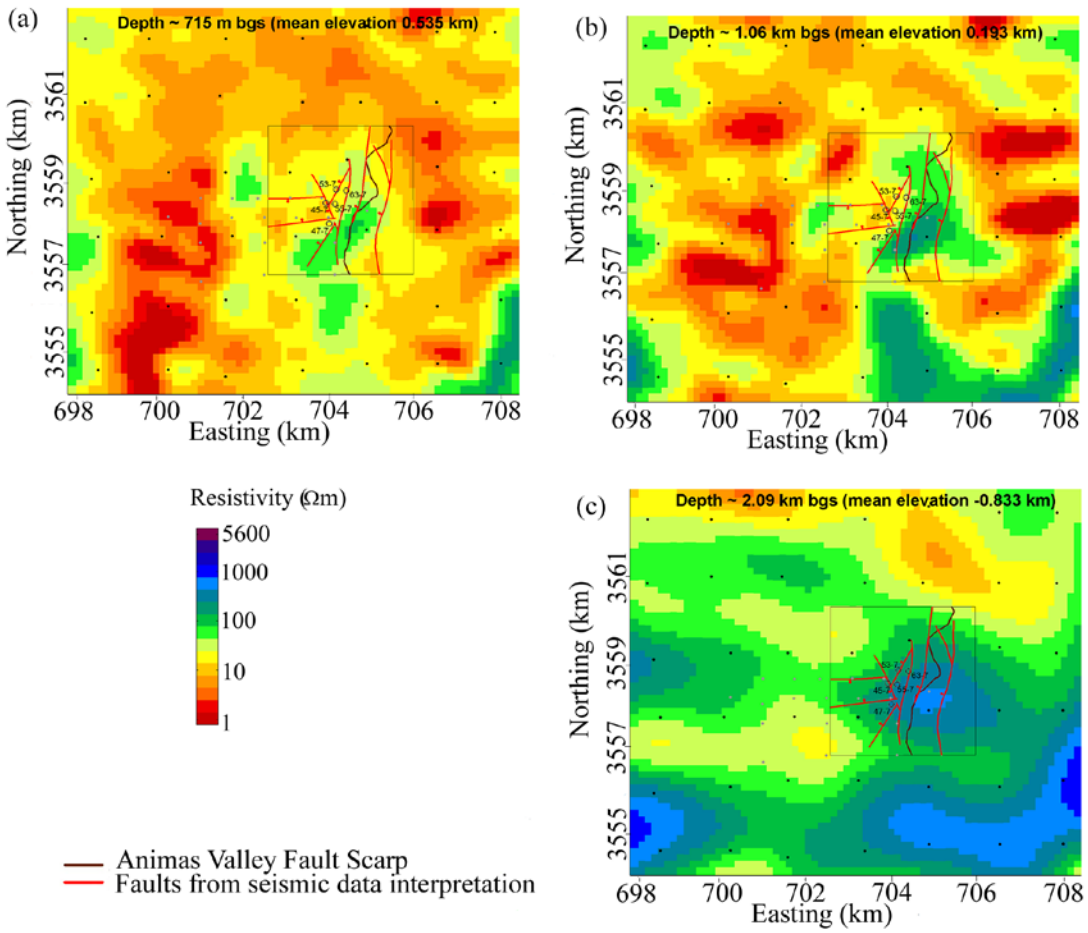

Fig. 3.2.4. Plan view of the inversion model at depths of (a) 715 m, (b) 1.06 km and (c) 2.09 km.

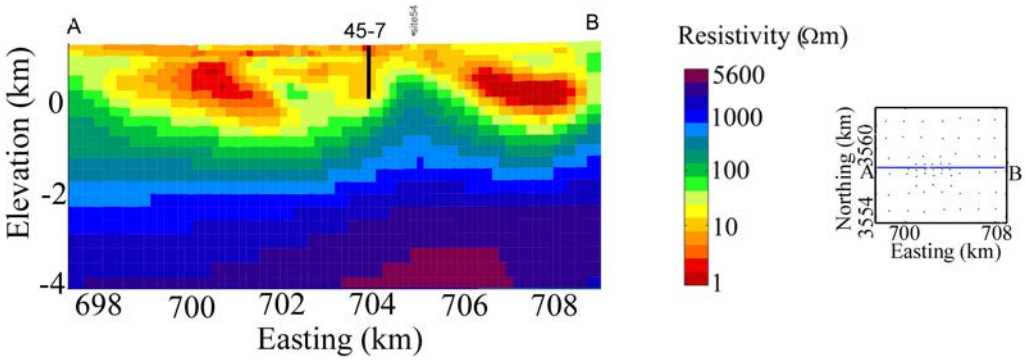

Fig. 3.2.4. East-west resistivity slice through productive well 45-7. The resistive horst block (green) and adjacent low resistivity basins are clearly imaged. The transition from low- to high-resistivity at the margins of the horst block are interpreted to contain fault zones. Productive well 45-7 was drilled into the steeply dipping fault zone on the western edge of the block. The low resistivities at the top of the horst block are interpreted to result from a combination of alteration and the shallow outflow plume of geothermal fluids encountered in the shallow wells.

3.3. Thermo Hot Springs

Thermo Hot Springs, UT, like Lightning Dock, is a moderate-temperature geothermal system developed primarily in Mesozoic carbonate rocks and sandstones (Fig. 3.3.1). The surface manifestations consist of silicified alluvium and hot springs. The reservoir is developed in Mesozoic sandstone and upper Paleozoic limestone and sandstone that overlie Precambrian metamorphic rocks and Tertiary granite. The reservoir rocks are overlain by Tertiary volcanic rocks. Beginning in November, 2007, Raser Technologies (now Cyrq Energy) drilled a series of wells south of the hot springs, the deepest being 17-34 (2835 m MD). The wells produce fluids sufficient for the generation of 10.5 MWe. Temperatures as high as 172°C have been encountered at depth. However, the temperature profiles suggest a dominantly conductive thermal regime, indicating the wells were not drilled in the main part of an upwelling zone.

Permeability at Thermo Hot Springs occurs within the carbonate rocks encountered in the wells. Fluid flow is interpreted to be fracture controlled; no evidence of karst topography or dissolution features has been recognized. The two wells discussed in this report are representative of the production wells. Most of the permeability is found below a depth of 900 m within the limestones. An XRMI scanner log was acquired in the lower part of 17-34 between 2335 and 2673 m (7660 and 8623 ft). This portion of the well encountered the lower part of the Redwall Limestone, skarn and metamorphic rocks. Six faults were encountered in this part of the well. The faults dip west to southeast between 22° and 72° and five of the six strike northeast to northwest; the remaining fault strikes east-west. Most of the open fractures encountered in the well are steeply dipping and strike northward.

Based on the presence of sheared skarn and rotation of the layering in the lower part of the Redwall Limestone, Anderson (2012) concluded that the limestone and skarn were separated from the underlying metamorphic rocks by a low-angle normal or “detachment fault”. He suggested the primary fluid reservoir at Thermo Hot Springs lies below this detachment fault and that upward fluid flow occurs where high-angle normal faults penetrate into the detachment fault zone.

Oxygen Isotope Data

Oxygen isotope measurements were made on 59 whole-rock samples from two of the productive wells, 13a-34 and 63-33, at the University of Utah’s SIRFER laboratory. The isotope and temperature data for these wells are shown in Figure 3.3.2. For reference, $\delta^{18}O$ values (~27 ‰) are consistent with the $\delta^{18}O$ value (+23 ‰ to +26 ‰) of unaltered marine carbonate rocks (Rao, 1990). Both wells show multiple zones of oxygen isotope depletion.

The temperature profile for 13a-34 suggests permeable zones are present at 1036 and 1494 m. The depths correspond approximately to zones of isotopically depleted rocks. A third zone of isotope depletion occurs at a depth ~1900 m. There is a subtle temperature increase at this depth, suggesting this may also be a permeable zone.

The rocks in well 63-33 display a different isotopic pattern. In this well, isotopically depleted rocks occur at 1100 m and below about 1500 m. The temperature profile is consistent with permeable zones at 1250 m and below 1500 m (compare the profile with 13a-34) but the survey data appears to be of marginal quality. Spinner surveys are required to confidently identify the permeable zones in this well.

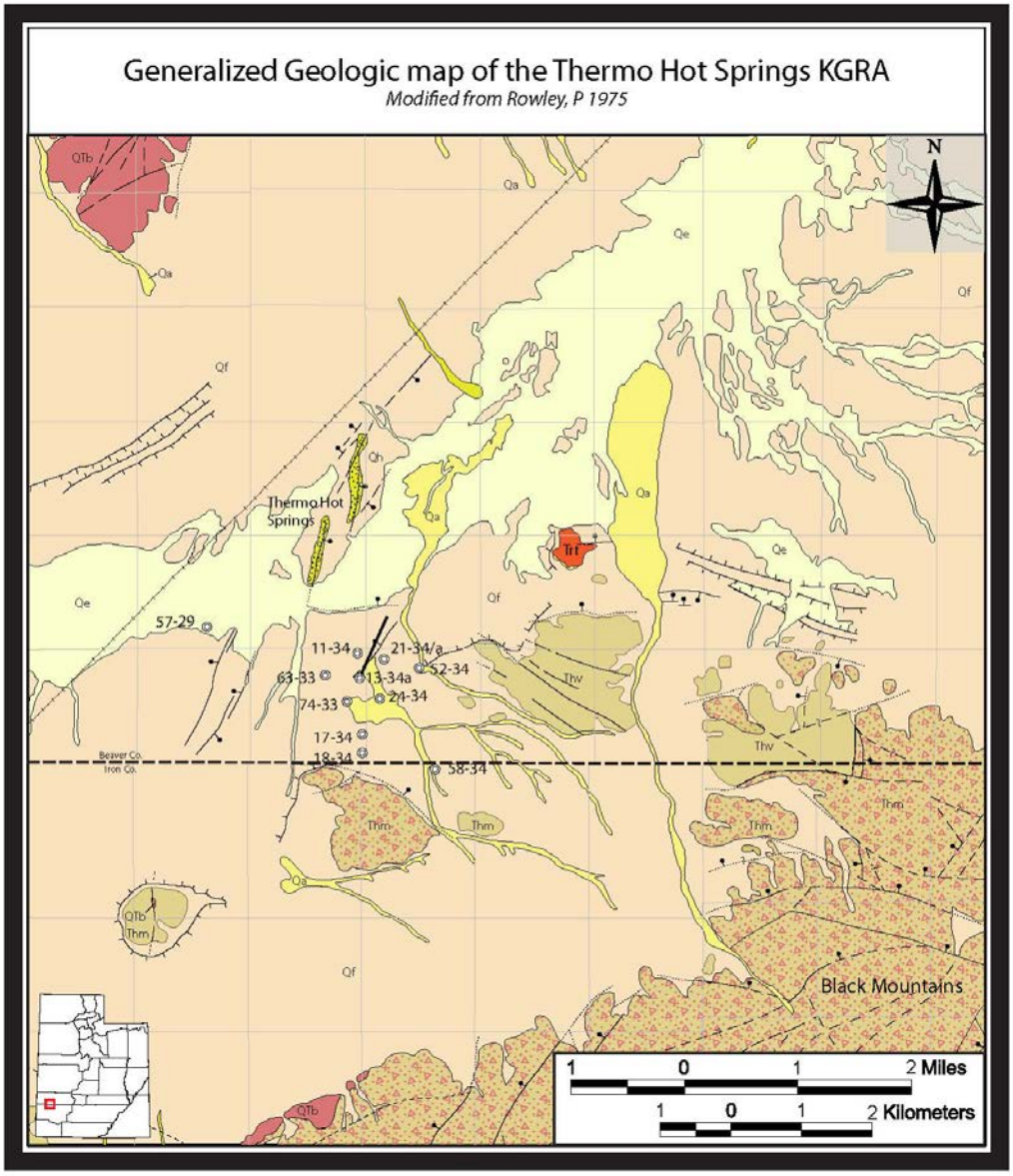

Fig. 3.3.1. Geologic map of the Thermo Hot Springs area (Rowley, 1978). Qa = Quaternary alluvium. Qf = Quaternary fan and pediment deposits. Qe = Quaternary Lake Bonneville deposits. Qh = hot springs deposits. Qtb = Quaternary/Tertiary basalt lava flows. Trt = Rhyolite of Thermo Hot Springs (Miocene). Thv = Horse Valley Formation (Miocene). Thm = Mafic member of the Horse Valley Formation (Miocene). * = probable eruptive center. Scale is approximately 1:79,200.

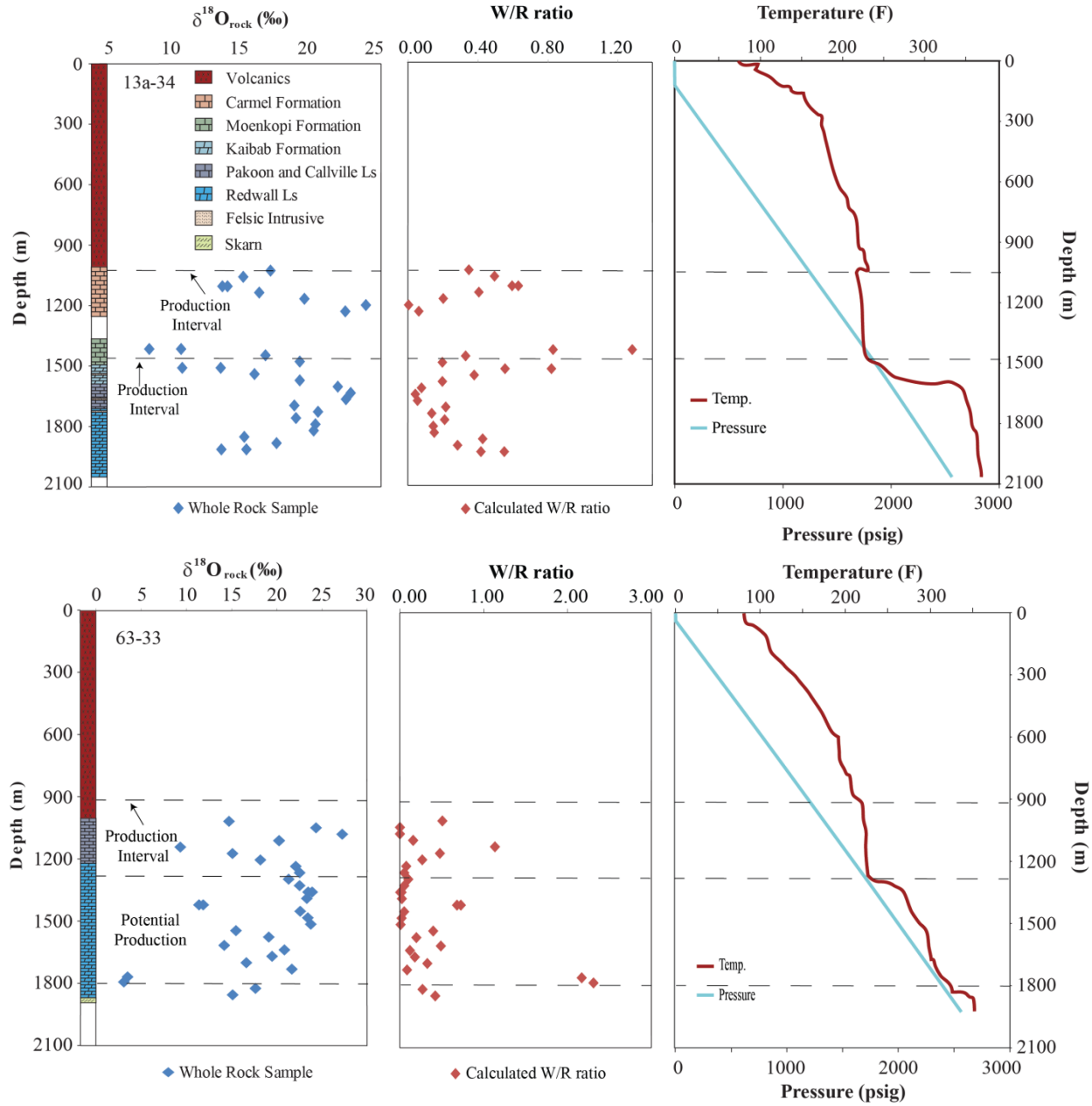

Fig. 3.3.2. Measured $\delta^{18}O$ values, temperatures, pressures and rock types vs. depth for production wells 13a-34 and 63-33.

MT Data

In 2010, Quantec Geoscience Inc. collected 90 MT soundings, on average 4 km apart, encompassing the well field (Fig. 3.3.3). Because of the presence of an active railway track and the 1.5 GW Delta IPP DC transmission line passing through the geothermal field from north to south, an ultra-distant remote reference was established for the survey in Buena Vista Valley in northwestern Nevada. This reference was effective in cancelling artificial noise and high-quality MT responses were obtained.

Plan maps of the recovered resistivity model at two depths, one near surface and the second at the approximate base of the wells are shown in Fig. 3.3.4. North-south and east-west cross sections are shown in Figure 3.3.5. A 3D view of the resistivity model approximately 1 km below the base of the wells is illustrated in Figure 3.3.6. The near surface plan map shows that the hot springs are located on a resistivity low that extends southward, along the trend of the hot springs fault. With increasing depth, the resistive basement rocks become increasingly prominent to the south.

The cross sections show that the low resistivities prominent in the near surface plan maps have limited vertical extents, suggesting they represent shallow clay-filled basins. Based on gravity data, the deepest basins extend to depths of about 2 km (elevations of 0 km) (Hardwick, 2013). Low resistivities (<100 ohm.m) at greater depths are interpreted to lie within the basement rocks. Thus, the moderate resistivities encountered at depths of 5-6 km (-3 km elevation; Fig. 3.3.6) in the southwestern part of the survey area are cannot be explained by thick clay deposits.

The Cyrq well field is located on the southern edge of the resistive block that is apparent in the MT maps below a depth of about 1 km. Gravity data support the conclusion that the high resistivities represent a horst block that we infer is bounded on its east and west sides by faults. No low-resistivity, pipe-like features that could be related to upflow zones in the immediate vicinity of the well field were detected.

The MT data indicate the presence of low resistivities immediately south of the well field (Fig. 3.3.4 at -0.4 and 3.3.5; north south section) below the clay cap, and a deeper region of moderate resistivities at the southwestern end of the mapped area (elevations of -2 to -4 km). These low resistivities define a northeast-trending belt between two resistivity highs. We suggest these deep, low to moderate resistivities are caused by an interconnected fracture network that forms the permeable fluid pathway connecting the deep geothermal fluids to the hot springs from the southwest.

Results of the Thermo study are consistent with our opening hypothesis. Oxygen isotope depletion of wellbore cuttings accompanies higher measured permeability and production. A low-resistivity lineation resolved by the MT entering to the geothermal field from the southwest does not appear to have an unconsolidated sedimentary cause. Not knowing temperatures precisely within this lineation, a contribution by low-temperature clays cannot be overruled. However, such clays also are consistent with a low to moderate temperature geothermal fluid flow.

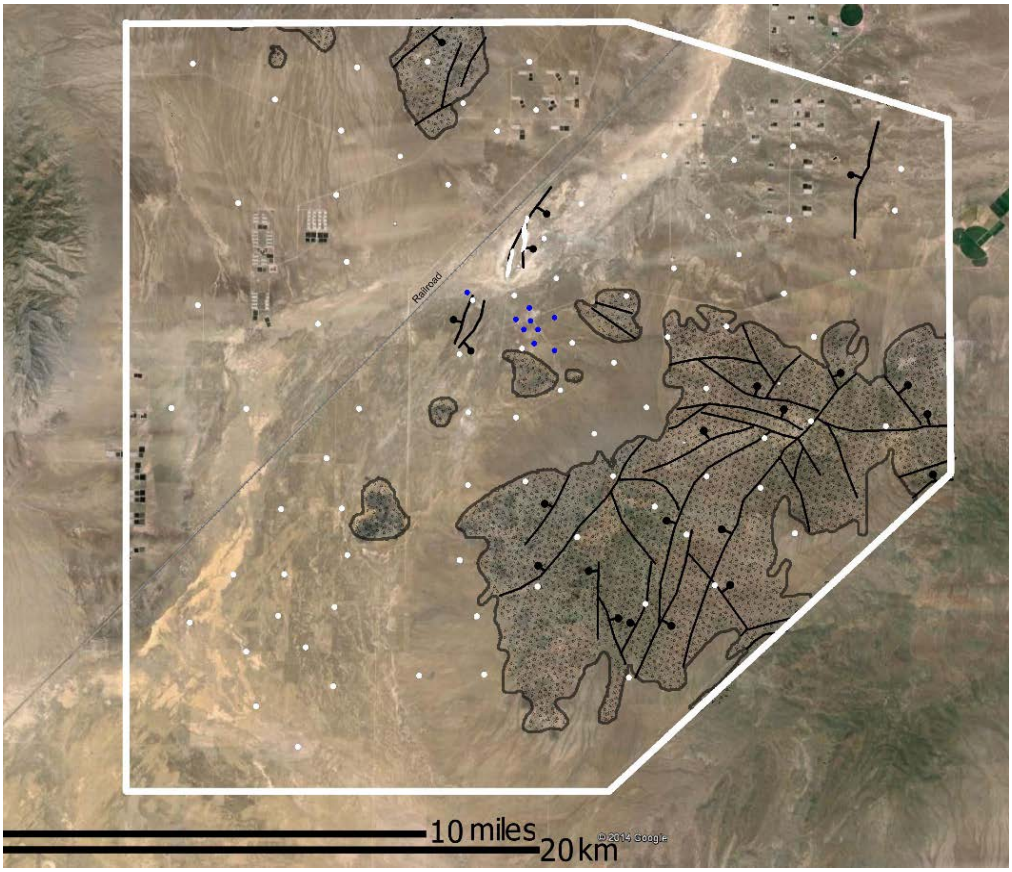

Fig. 3.3.3. Map of the survey area showing the MT station locations 1 to 90, and geothermal wells (blue dots).

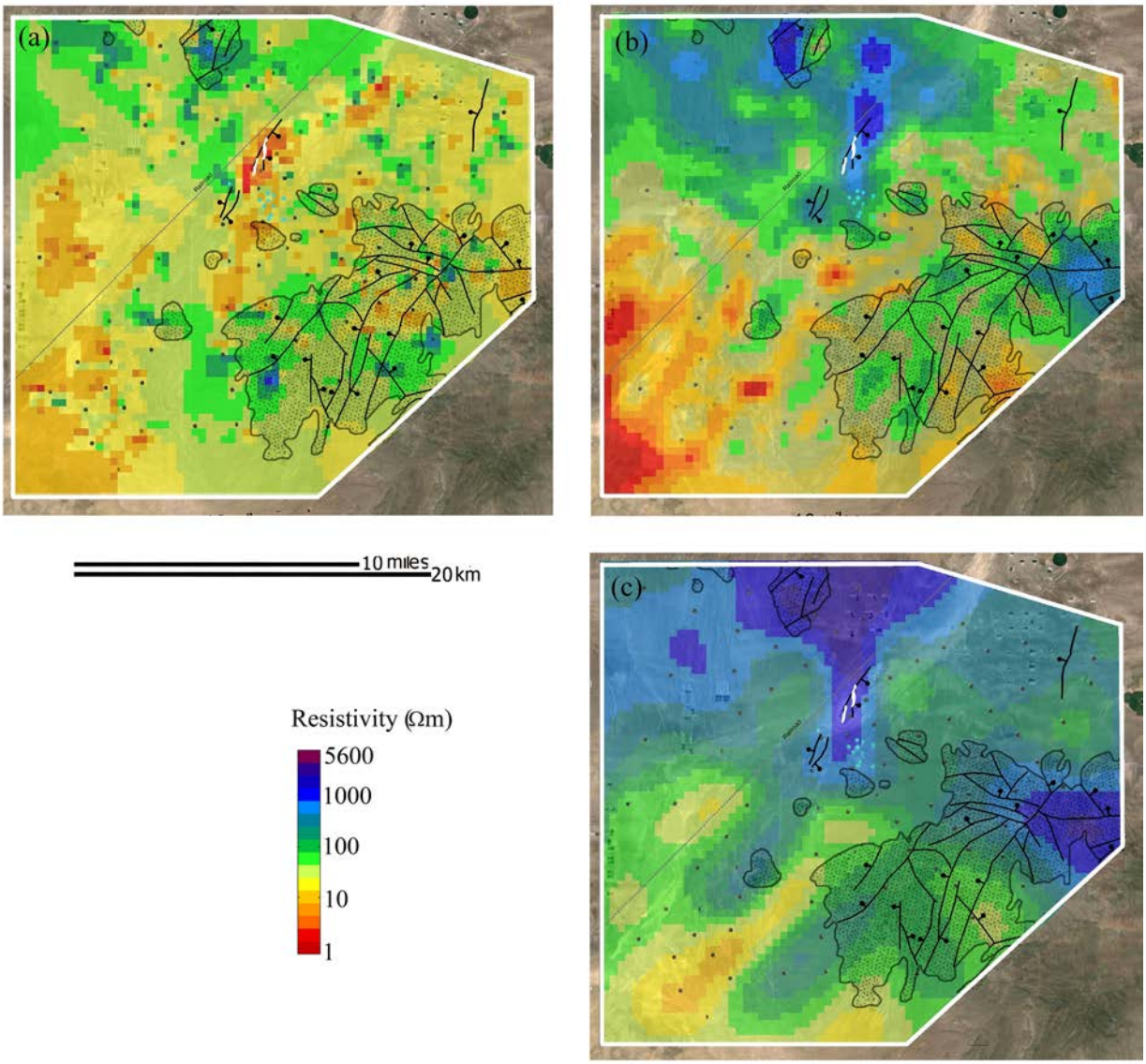

Fig. 3.3.4. Plan views of the resistivity model at elevations of 1.4 (a), 0.4 (b) and at -0.9 (c) km asl. Faults in the Black Mountains are shown with the ball on the downthrown side.

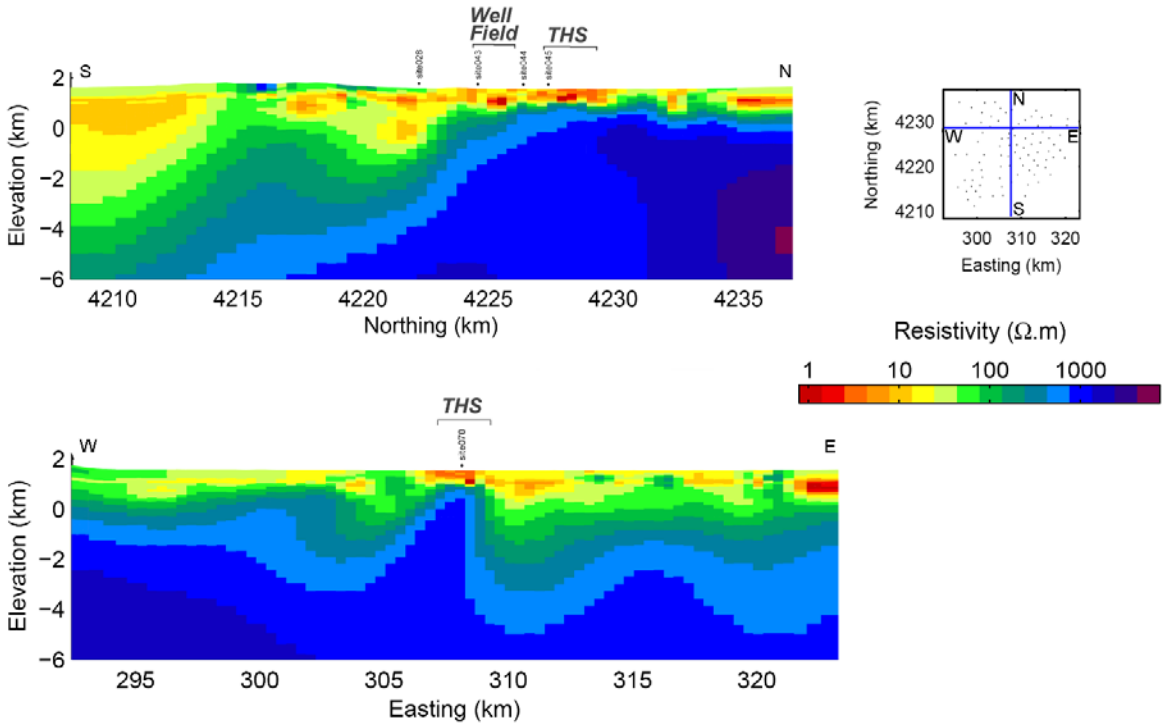

Fig. 3.3.5. North-south (upper) and east-west (lower) resistivity slices through Thermo Hot Springs (THS). The strong resistivity contrast on the edges of the horst block below THS are interpreted as faults.

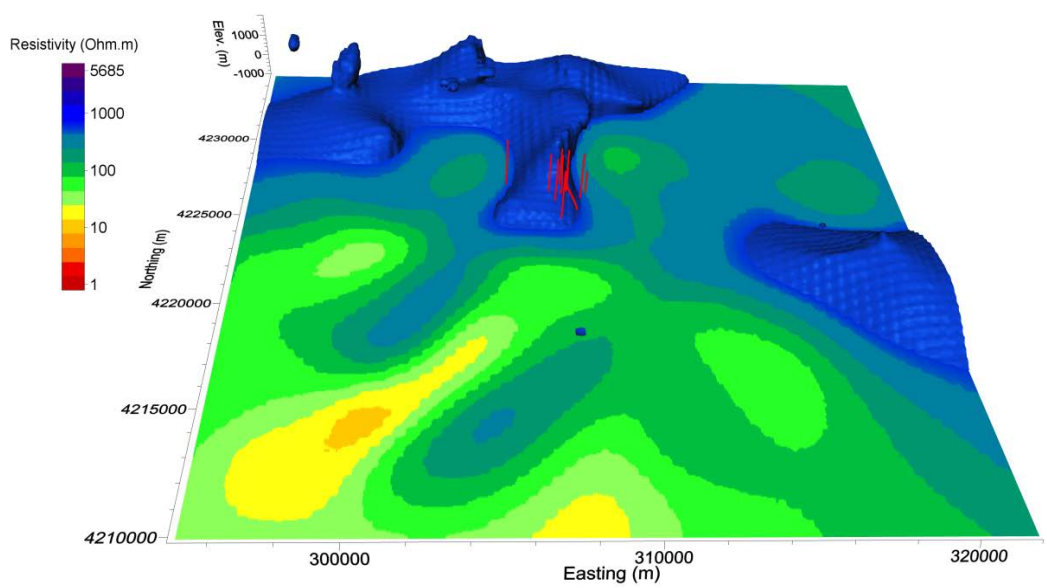

Fig. 3.3.6. Plan view at -1 km elevation through the resistivity model, with the traces of geothermal wells shown in red and an iso-surface corresponding to 600 ohm.m (dark blue areas). The east, west and southern boundaries of the horst block appear to be bounded by faults. A possible geothermal fluid conduit is interpreted to enter the system from the southwest corner of this plan view.

3.4. Raft River Geothermal Field, Idaho

The Raft River geothermal system is located in the Raft River Valley, Idaho, a north-trending Cenozoic basin on the northern edge of the Great Basin (Fig. 3.4.1). U.S. Geothermal operates a 13 MW net capacity power plant at the site. Raft River was included in this study because the field has been intensely studied under the DOE/EERE EGS project "Concept testing and development of the Raft River geothermal field, Idaho". As part of the EGS project, new MT data were acquired. No isotopic data, however, were collected.

The geothermal reservoir at Raft River is developed in Precambrian metamorphic rocks that underlie approximately 1500 m of Tertiary and Quaternary volcanic and volcaniclastic deposits. The primary reservoir host rock is the Elba Quartzite, although the underlying quartz monzonite can also be productive (e.g. RRG-7). Figure 3.4.1 shows the locations of the injection and production wells. The maximum temperatures encountered in the reservoir are close to 150°C. Smectite is the stable clay mineral at this temperature and minor amounts have been found throughout the wells.

Chemical analyses of the geothermal waters has shown that those from the northwest wells are distinctly less saline than those produced from the southeast wells although both groups of fluids are produced from the metamorphic rocks and appear to have the same thermal histories (Ayling and Moore, 2013). These differences imply the presence of a hydraulic barrier between the two groups of wells. This barrier is interpreted to be a shear zone. It is informally referred to

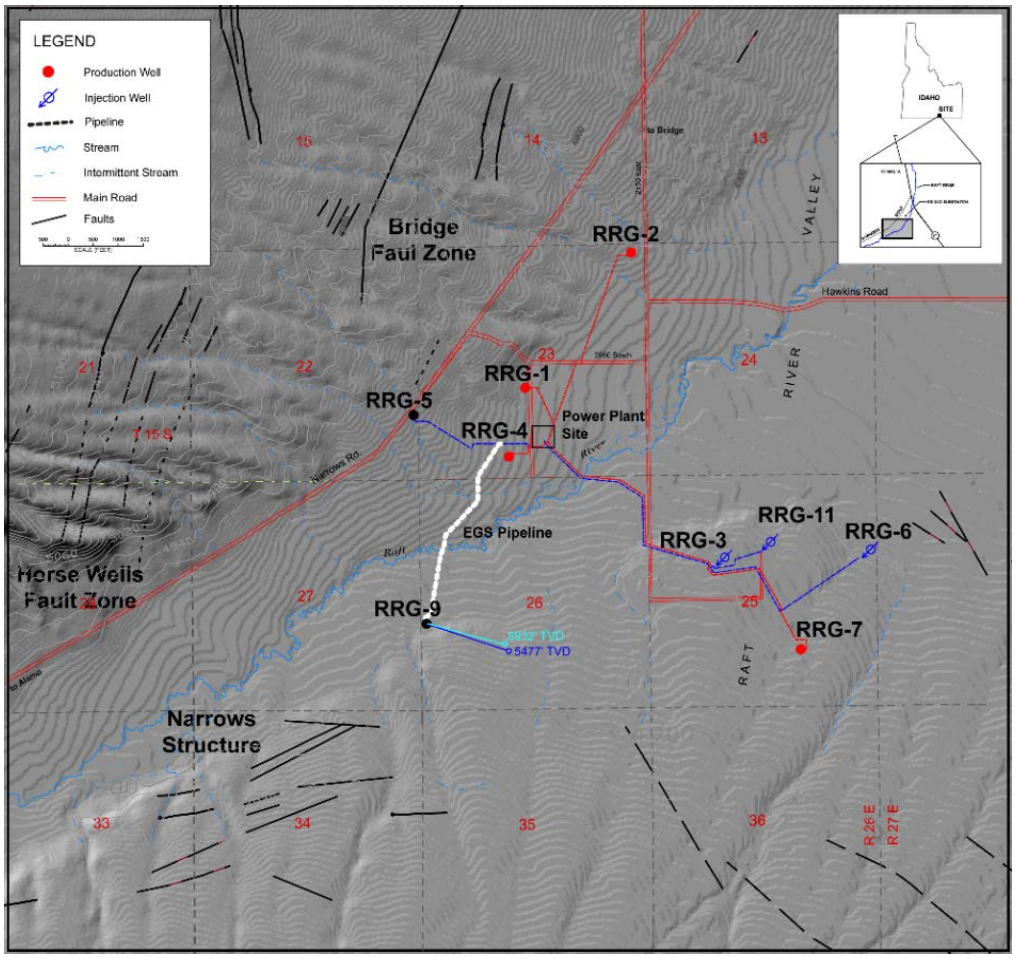

Fig. 3.4.1. Locations of the geothermal wells and faults cutting the alluvium. The white line is the pipeline connecting the plant to RRG-9 ST1 (Side-track 1 of RRG-9 with a TVD of 5477 ft) as the Narrows Zone. Well data suggests there is no disruption of the Precambrian-Tertiary contact across the field; thus the Narrows Zone does not extend upward through the Tertiary rocks.

Permeability within the reservoir is fracture controlled. Televiewer surveys of RRG-9 ST1 indicate that the fractures in the Elba Quartzite are steeply dipping and that the majority strike northeast. Within the Precambrian rocks, microearthquakes define a region of fractures several hundred meters wide that extends northeastward from RRG-9 ST1 through the well field (Fig. 3.4.2). Since August 2010, approximately 150 earthquakes have been recorded with magnitudes ranging from -.3 to 1.5. This zone is interpreted to represent fractured rocks located on the southeast edge of the Narrows Zone.

Oxygen Isotope Data

No whole-rock isotopic analyses were performed.

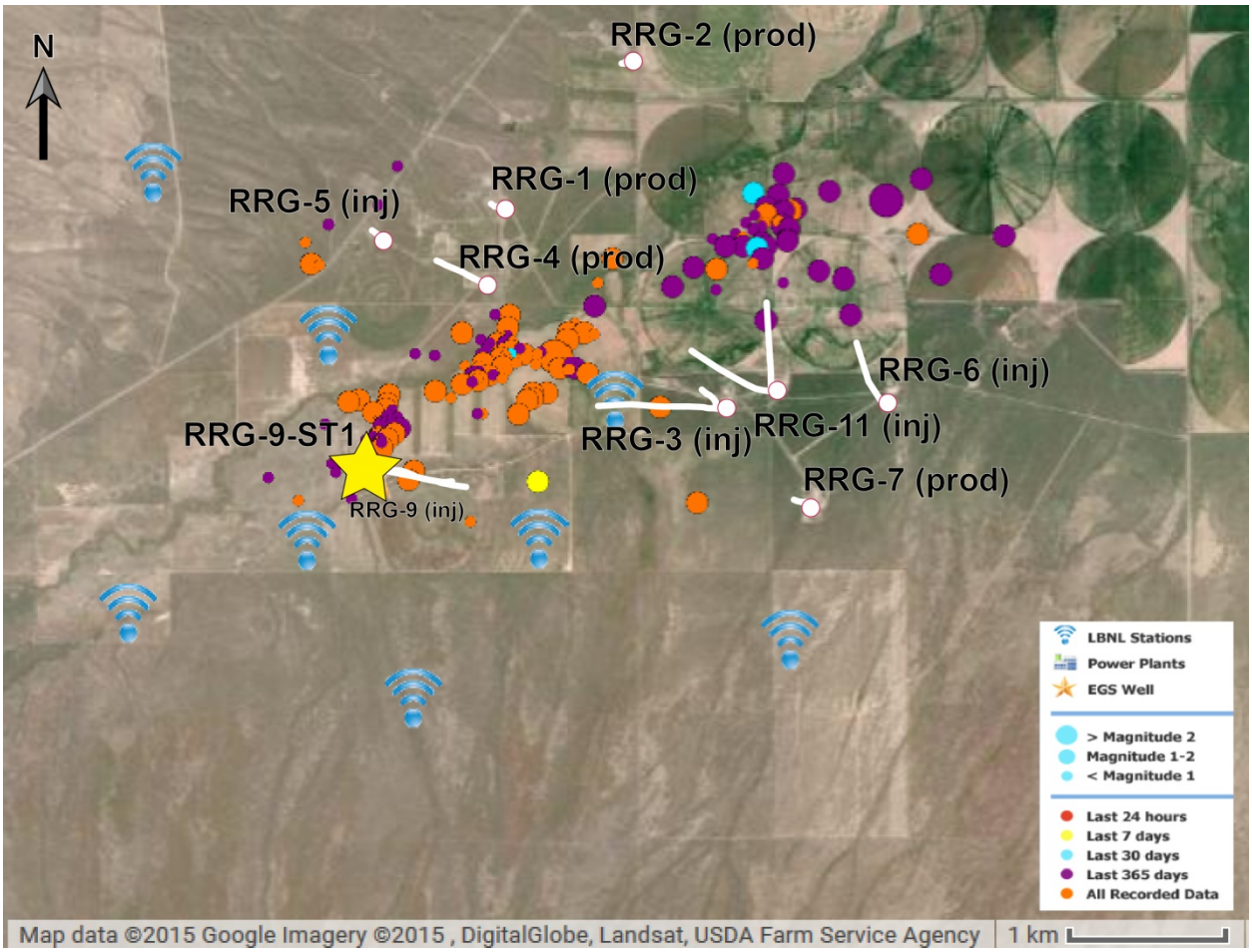

Fig. 3.4.2. Locations of microearthquakes since August, 2010. Well tracks are shown by the white lines, seismic stations by the antenna. The stations are monitored by Lawrence Berkeley National Laboratory, under the direction of E. Majers.

MT Data

In 2011, 105 MT soundings spaced 0.5 to 1 km apart were collected by Quantec Geoscience Inc, with the highest density near the well field (Fig. 3.4.3). The 3D resistivity distributions with respect to the well locations and depth are shown in 3.4.4. Near surface low resistivities reflect the argillic alteration of the volcanic and volcaniclastic rocks. The lower two plan maps show resistivities within the Precambrian rocks. The most significant feature of these deep plan views is the northwest-trending low resistivity region extending across the productive portion of the field. The low resistivities extend downward to at least several kilometers depth (Fig. 3.4.5). The coincidence of this feature with the productive wells suggest it represents a fluid conduit. This conductor is relatively more developed toward its southeast end which may correlate with the higher salinities in well fluids in that direction. RRG-9 ST1 is located in resistive rocks, southwest of the permeable fairway, consistent with its low permeability.

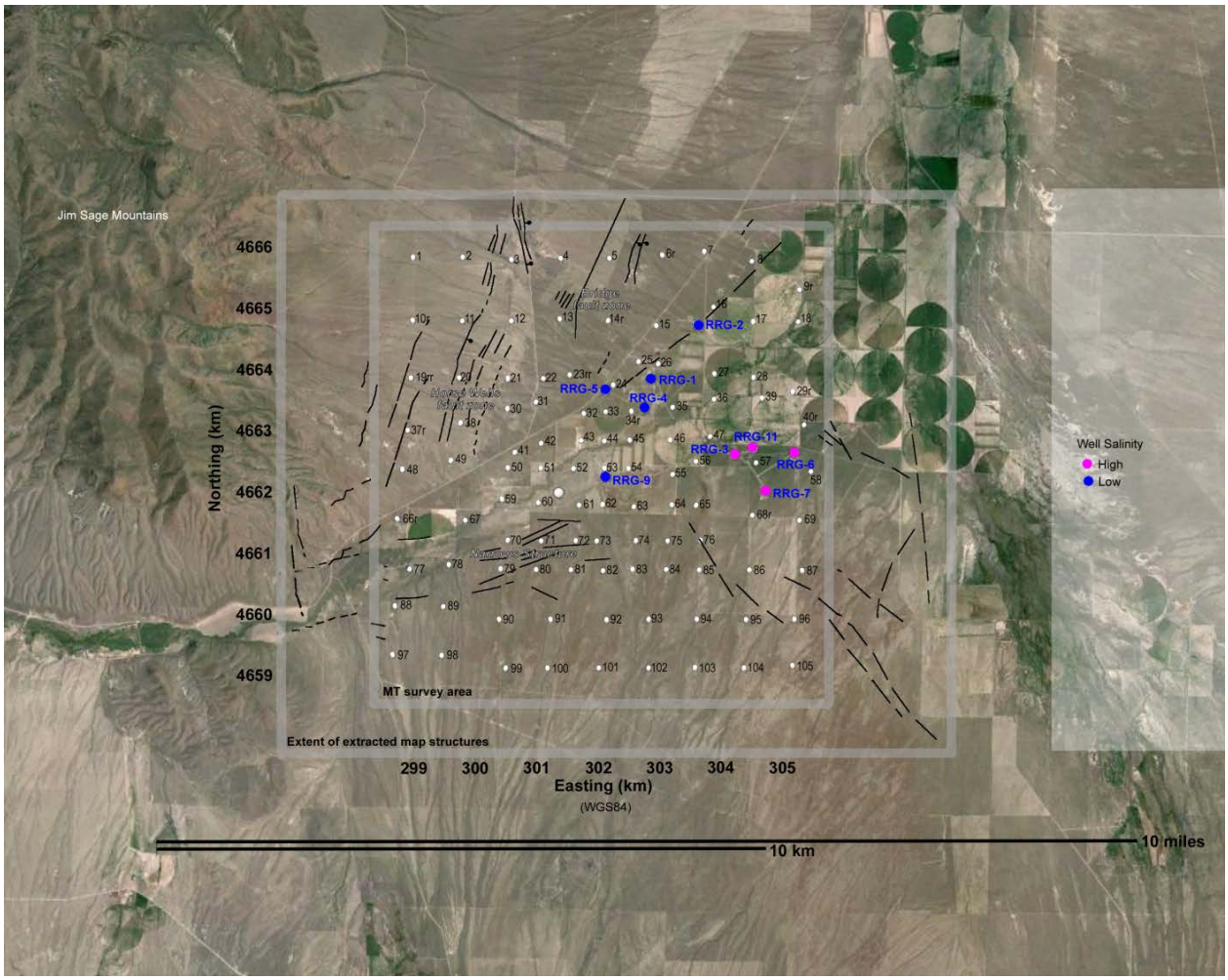

Fig. 3.4.3. MT sounding locations, geothermal wells, colored according to whether they produce high or low salinity geothermal waters (Ayling and Moore, 2013), and mapped faults overlaid on Google Earth image.

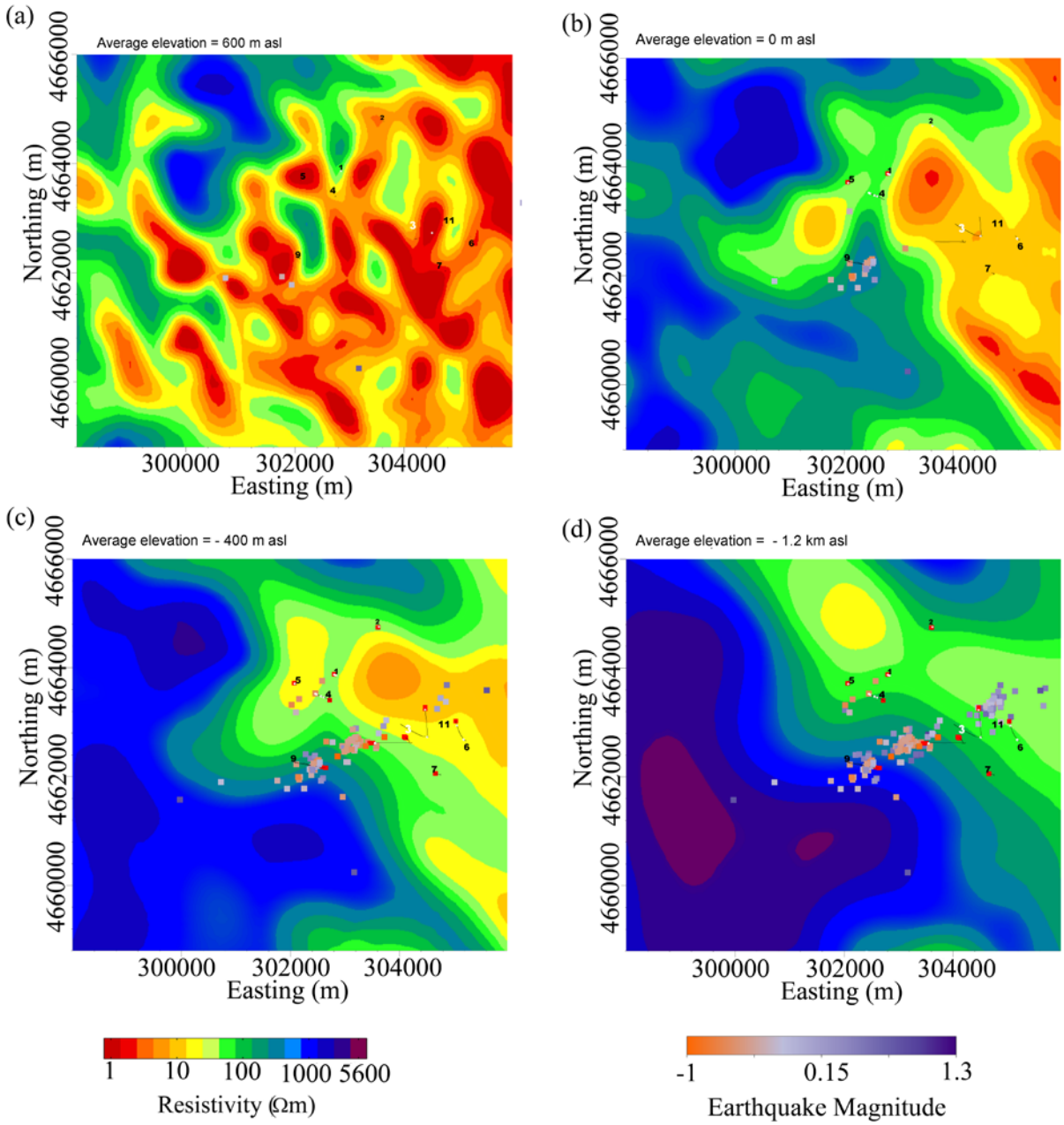

Fig. 3.4.4. Distribution of resistivities, wells, microearthquakes and mapped faults at elevations of (a) 600 m; (b) 0 m; (c) -400 m, - and (d) -1.2 km asl. Only microearthquakes occurring above the depth of the plan map are shown. The top of the Precambrian is located at approximately 0 m elevation.

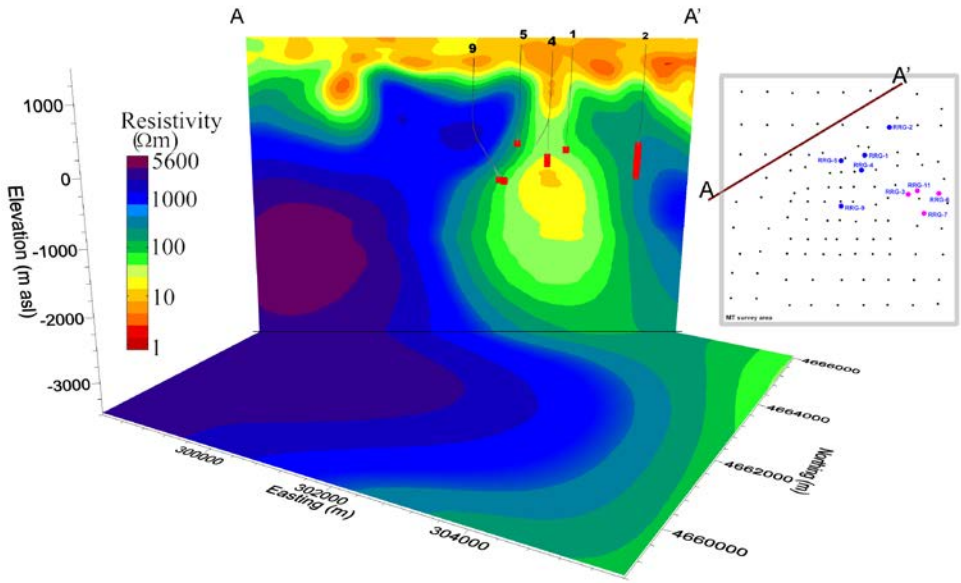

Fig. 3.4.5. Distribution of resistivities in the vicinity of the production wells. The red socks on the wells indicate Precambrian rocks, which are located at a depth of 0 m asl.

Application of Isotope and Electrical Resistivity Data to Permeability Mapping

Evaluation of oxygen isotope and resistivity data demonstrates that both provide information on reservoir permeabilities, although at different scales. The locations of isotopically depleted rocks at the wellbore scale coincides with the locations of commercial production zones at Coso Hot Springs and Thermo Hot Springs. These isotopic depletions are indicative of high water-rock ratios. At Lightning Dock, there is no evidence of isotopic depletions in the “dry” holes.

Interpretation of the water-rock ratios, based on the isotope depletions, suggests extensive interactions between the fluids and rocks, and that these fracture zones have been conduits for significant periods of time. Reconnaissance surveys conducted on well cuttings from Coso Hot Springs show broad areas of isotopic depletion and evidence of field-wide gradients in water-rock ratios. The lowest isotopic values (highest water-rock ratios) correspond to areas of high reservoir permeability.

We have also demonstrated that MT surveys can be an effective tool for understanding and mapping reservoir-scale permeability in both high- and moderate-temperature geothermal systems, and that the geometries of low resistivity zones can be used to distinguish clay caps from regions of high permeability. At all four systems, the low resistivity zones interpreted to be clay caps or clay-filled basins lack roots that could connect them to deeper, steeply dipping conduits representing the upflow zones. Deep, fluid-bearing conduits are most clearly imaged at Coso Hot Springs and Raft River. At Coso Hot Springs, the clay cap is relatively thin and coincident with the distribution of smectite and conductive thermal gradients. Wannamaker, in Moore et al. (2008), shows an example of a thicker, low-resistivity clay cap in the volcanic-hosted system at Karaha-Telaga Bodas.

In low- to moderate-temperature systems, where temperatures are less than about 200ºC, smectite can be stable throughout the reservoir and in the surrounding areas, potentially producing large regions of low resistivities. These can be quite thick, up to several kilometers deep, within basin interiors where faulting and large-scale down warping can occur. An example of these deep basins is found at Lightning Dock. These regions of low resistivity are not rooted.

The best example of a deeply rooted moderate-temperature system is found at Raft River. The roots appear to be relatively narrow zones within otherwise resistive rock. Drillhole data suggest this is not due to changes in rock type. Although smectite may be present in these zones at depth, the more likely explanation is that they represent regions of interconnected fractures containing geothermal fluids. At Lightning Dock, the single productive will is located within a deep relatively isolated resistivity low, along a nearly vertically oriented change in resistivity. The resistivity low is interpreted to represent a relatively narrow, highly fractured region in the upper part of the fault. At depth, flow may be more diffuse. At Thermo Hot Springs, there is no evidence of a pipe-like upflow zone below the well field, consistent with temperature data suggesting the well field is not located within the main upflow zone. The fluid source zone is interpreted to be located southwest of the well field, where deep low resistivities are observed, so that fluids are entering laterally rather than vertically.

The Phase I data documents important similarities between the fields, as well as showing that each field has its own unique characteristics that must be interpreted in light of other geologic, geochemical and geophysical data. We believe it is important to point out that the moderate-temperature fields examined in Phase I all produce less than 15 MWe. These are relatively small fields compared to Steamboat Hot Springs (~100 MWe), Dixie Valley (~60) and McGinness Hills (~70 MWe). These larger fields can be expected to have more extensive and better developed signatures and be more appropriate targets when searching for blind systems. Examining such a system is considered under our recommendation for Phase II work.

In summary, the results of Phase I demonstrate that useful information on reservoir permeability can be obtained at relatively low cost from drill samples such as those collected during routine slim hole or gradient drilling. Complementary mineral investigations, conducted using thin sections and X-ray diffractometry provide information on clay distributions. Such information is necessary for the interpretation of the MT data, temperature, fluid type, and the locations of fracture and permeable reservoir features. Oxygen isotope data collected on the rocks can provide both regional and local information on the extent of water-rock interactions and reservoir permeability using the procedures outlined in Task 1. These data, when integrated with resistivity models developed using the procedures and algorithms described in Task 2 (and other geological, geochemical and geophysical studies) provide a powerful tool for mapping large areas of high geothermal potential with significantly greater confidence than we currently have. Analysis of additional geothermal systems, ideally those with significant productivity, will increase confidence in assigning physical and chemical conditions to MT geophysical structure.

Task 4.0. Analysis and Validation

State of the art 2011 exploration costs and widely observed exploration success rates as seen by the industry will be used to construct a baseline for Levelized Cost of Electricity (LCOE) analysis. The reduction in exploration risk using the new technology proposed here will be quantified and the cost components will be used to model Geothermal Electrical Technologies Evaluation Model (GETEM) cases thereby evaluating the % reductions in LCOE (from baseline) that can be achieved.

The primary objective of this project is to improve drilling success rates utilizing relatively low cost exploration techniques. Figure 4.0.1 shows the effect of improving success rates on the Levelized Cost of Electricity (LCOE) for 150° and 175°C resources. This range of temperatures is typical of the conditions encountered in low- to moderate- temperature resources similar to those investigated in this project. These generation cost estimates assume that exploration and confirmation drilling occur at a single site where the cost of exploration drilling will be $3M and three successful confirmation wells are required. It is assumed these wells are 6000 ft in depth and that they will produce at a pumped rate of 2000 gpm. The curves show the effect of improving drilling success rates from 40 to 100% for both the confirmation phase and for the entire well field. These cost estimates include both royalties, taxes and insurance, which account for ~$0.008 per kW-hr. It is apparent that even minor improvements in the confirmation success rate have a significant effect on the LCOE.

These estimated LCOE's are based upon a discount rate of 30% during the exploration and confirmation phases. With an increased drilling success, there is an increased likelihood that the financing costs during the confirmation phase might be reduced, which would provide further reductions in the LCOE. As an example, for the scenario where the success rates are 60% for confirmation and 80% for the well field, lowering this discount rate from 30% to 20%, would lower the LCOE by ~$0.0065 per kW-hr for both of these resource temperatures. The degree to which the discount rate would change is conjecture, however there is probability that it would decrease. This suggests the values shown in figures 4.0.1 are conservative estimates of the degree to which improved confirmation drilling success would lower the LCOE.

Go/No-Go/Redirect Decision

Upon completion of Phase I, a review will be conducted of the developed procedures and of the analyzed results from the two systems proposed to be studied, and a Go/No-Go/Redirect decision will be made by the Department of Energy (DOE) prior to proceeding to Phase II. This decision will be based on the following:

(i) Completion of a Phase I Report documenting the results of the Phase I tasks; the verification of the relationship between reservoir permeabilities, degree and type of clay alteration, and temperature to the electrical resistivities using the in-house 3-D modeling; and the rationale for continuing into Phase II;

(ii) Demonstration that the remaining budget and cost share are adequate to complete the remaining tasks; and

(iii) When applicable, documentation of the permitting, site access, and environmental documentation needed for Phase II. Include an assessment of whether the permitting, site access, and environmental documentation will be achievable within the remaining budget and timeframe.

Phase 1 has met the criteria established for a positive Go/No Go Decision. (i) We have verified a relationship between permeability, clay alteration, temperature and resistivity. (ii) The remaining portion of the proposed budget is adequate to conduct additional investigations of another geothermal system as planned under Phase II. (iii) No field work or permitting will be required to conduct these investigations.

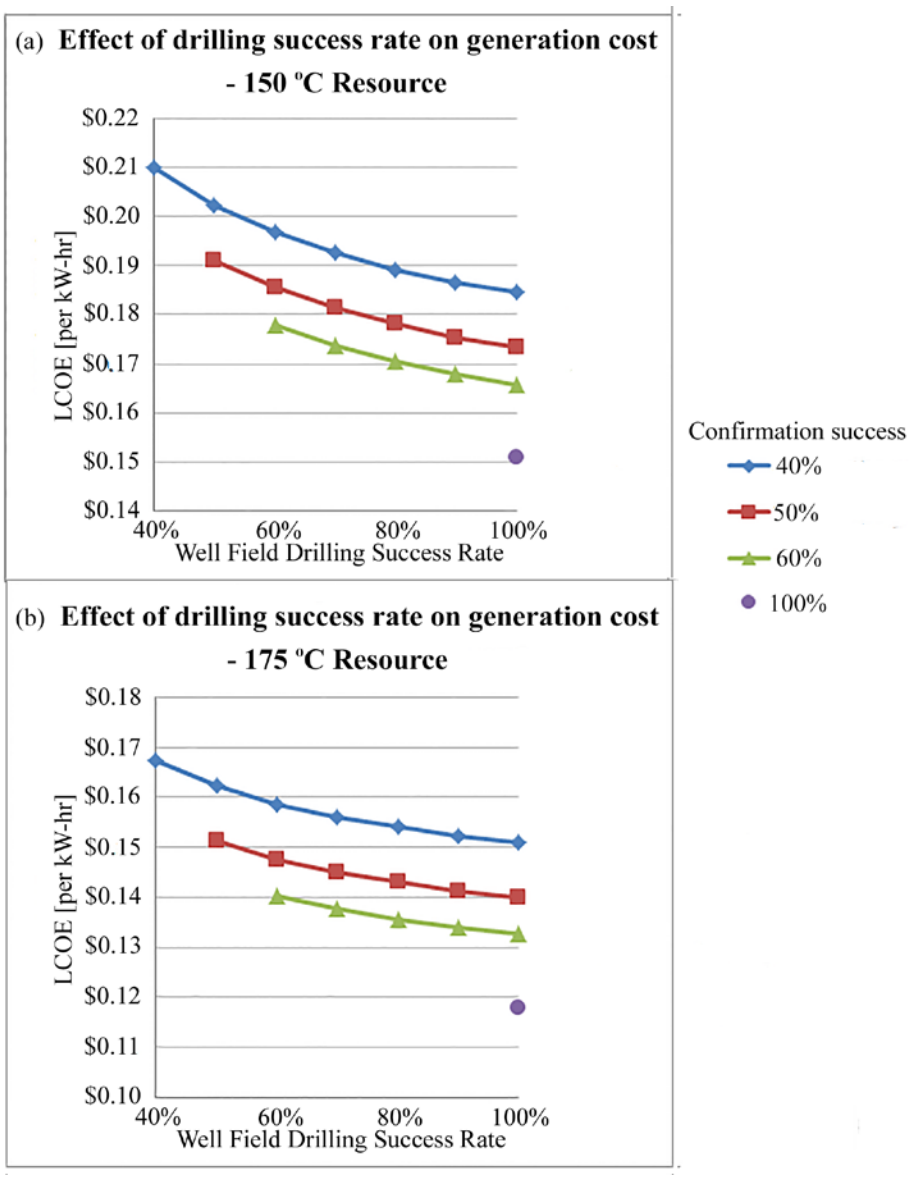

Figure 4.0.1. The effect of the drilling success rate on the LCOE for (a) a 150°C resource and (b) a 175°C resource. These costs were estimated using GETEM.

PHASE II –Validation

In Phase II, the framework and procedures developed in Phase I will be validated using the MT data and the interpretational framework and procedures established in Phase I.

Task 5.0. Sample Collection and Analyses

Samples and data will be collected from existing wells for X-ray diffraction, petrographic and oxygen isotopic analyses. The samples will be analyzed and interpreted following the procedures outlined under Phase I.

In our original proposal, Coyote Canyon, NV, was advocated for study during Phase II. This field lies on the east side of the Stillwater Range approximately 5 km southwest of the producing field at Dixie Valley. Wells drilled to depths near 3000 m have encountered temperatures up to 285°C. The basement consists of Paleozoic and Mesozoic sandstone, siltstone and limestone and Mesozoic and Cenozoic gabbro, diorite and granodiorite. Terra-Gen has provided data from a dense, focused 3-D MT survey and cuttings samples. The area is geologically complex and is abutted by the thick, altered, and electrically conductive sediments of Dixie Valley. In light of this setting, and additional developments since original proposal submission, we will suggest a change in Phase II field area below.

Task 6.0. Validation of Framework and Procedures

We will validate the interpretational framework and procedures developed in Phase I. We will first use the MT data to predict the temperature and permeability distributions within the geothermal system. We will then confirm these predictions by comparing them to the results of the mineral and isotopic analyses and the well data.

It was anticipated that Terra-Gen would continue development activities at Coyote Canyon and that new data would be made available to the project. Unfortunately, the project is on hold and no further data collection is anticipated in the near future.

We have been approached by Ormat to consider an investigation of their McGinness Hills, NV geothermal project. By the end of 2015, the field will be producing 70 MWe, making it the second largest in Nevada after Steamboat Hot Springs and exceeding Dixie Valley. It can be anticipated that systems of this size will be associated with more extensive and better developed resistivity and isotope signatures than the apparently smaller geothermal systems investigated in Phase I.

These larger systems are, from an economic perspective, very attractive targets, particularly when searching for blind resources, which is one of the goals of this investigation.

Thus, understanding their signatures is critical. McGinness Hills was suggested to contain a deeply rooted fluid source based on transect MT of Wannamaker et al. (2011). High quality 3D MT data has been collected there now and is available for new inversion. Collection and integration of isotopic, mineralogical and MT data would allow us to predict the permeability structure of the system and then validate it with field data.

Task 7.0. Commercialization Roadmap

A detailed evaluation of all the possible commercialization options for the computational tools and the framework developed will be carried out. The best-suited option will be executed to transfer the technology developed into the commercial marketplace.

The University of Utah's Technology Commercialization Office will assist EGI in evaluating the commercialization potential after DOE funding and will pursue the most suitable avenues to license and/ or commercialize the technology thorough a start-up company based at the University of Utah.

Deliverables

Anderson, W. V., 2012. Implications of thrust and detachment faulting for the structural geology of the Thermo Hot Springs KGRA region, Beaver County, Utah, Thesis, University of Utah, Department of Geology and Geophysics, 92 p.

Etzel, T.M., Bowman, J.R., McCulloch, J.M., Moore, J.N., Spicuzza, M.J., and Valley, J.W., 2017, Oxygen isotopic evidence of water-rock interactions in the Coso geothermal system: Journal of Volcanology and Geothermal Research, v. 329, p. 54-68..

Etzel, T., 2015, Isotopic and mineralogic insights to water-rock interaction at Coso Hot Springs geothermal system, Thesis, University of Utah, Department of Geology and Geophysics, in prep.

Etzel, T.M., Bowman, J.R., McCulloch, J.M., Moore, J.N., Spicuzza, M.J., and Valley, J.W., 2013, Oxygen isotopic evidence of water-rock interactions in the Coso geothermal system: Proceedings, 38th Workshop on Geothermal Reservoir Engineering.

Simmons, S.F., Moore, J. N., and McCulloch, J., 2014, Assessment of fluid-mineral equilibria in the Coso geothermal reservoir: Proceedings of the 36th NZ Geothermal Workshop, Auckland, New Zealand, 4 pp.

REFERENCES

Ayling, B., and Moore, J.N, 2013, Fluid geochemistry at the Raft River geothermal field, Idaho, USA: New data and hydrogeological implications: Geothermics, v. 47, p. 116-126.

Ackerman, H.D., 1979, Seismic reflection study of the Raft River geothermal area, Idaho: Geophysics, v. 44, p. 216-225.

Bertrand, E. A., Caldwell, T.G., Hill, G.J., Wallin, E.L., Bennie, S.L., Cozens, N., Onacha, S. A., Ryan, G. A., Walter, C., Zaino, A., and Wameyo, P., 2012, Magnetotelluric imaging of upper-crustal convection plumes beneath the Taupo Volcanic Zone, New Zealand: Geophysical Research Letters, v. 39, p. 6, doi: 10.1029/2011GL050177.

Browne, P.R.L., 1978, Hydrothermal alteration in active geothermal fields: Ann. Rev. Earth Planet. Sci, v. 6, p. 229-250.

Chave, A. D., and A. G. Jones (eds), 2012, *The Magnetotelluric Method: Theory and Practice,* Cambridge University Press, Cambridge, 530 pp., 2012.

Covington, H.R., 1983, Structural evolution of the Raft River basin Idaho in Tectonic and Stratigraphic Studies in the Eastern Great Basin: Memoir 157, Geological Society of America, p. 229-237.

Criss, R.E. and Taylor, H.P. Jr., 1986, *Meteoric-hydrothermal systems* in Stable Isotopes in High Temperature Geological Processes, J.W. Valley, H.P. Taylor, Jr. and J.R. O'Neil (eds), Reviews in Mineralogy 16, 373-422.

Cumming, W., and Mackie, R., 2007, 3D MT Resistivity Imaging for Geothermal Resource Assessment and Environmental Mitigation at the Glass Mountain KGRA, California: Geothermal Resources Council Transactions, v. 31, p. 331–334.

Cumming W, and Mackie R, 2010, Resistivity imaging of geothermal resources using 1D, 2D and 3D MT inversion and TDEM static shift correction illustrated by a glass mountain case history. In: Proceedings, World Geothermal Congress, Bali, Indonesia.

Davatzes, N. E., and Hickman, S. H., 2006. Stress and faulting in the Coso geothermal field: update and results from the East Flank and Coso Wash: Proceedings of the 31st Workshop on Geothermal Reservoir Engineering Stanford University, 12 pp.

Giggenbach, W.F., 1988. Geothermal solute equilibria. Derivation of Na-K-Mg-Ca geoindicators. Geochimica et Cosmochimica Acta 52, 2749–2765.

Hardwick, C.L., 2013, Geothermal resources in southwestern Utah: Gravity and magnetotelluric investigations. (Master's Thesis) Department of Geology and Geophysics, The University of Utah, 1-56.

Jones, C., Moore, J., Teplow, W., and Craig, S., 2011, Geology and hydrothermal alteration of the Raft River geothermal system, Idaho: Proceedings, 36th Workshop on Geothermal Reservoir Engineering Stanford University, Stanford, California, January 31 - February 2, 2011, SGP-TR-191.

Kordy, M. A., P. E. Wannamaker, V. Maris, and E. Cherkaev, 2015, Three-dimensional magnetotelluric inversion including topography using deformed hexahedral edge finite elements and direct solvers parallelized on SMP computers: Geophys. J. Internat., in revis.

Kovac, K.M., Moore, J.N., and Lutz, S.J. (2005). Geologic Framework of the East Flank, Coso Geothermal Field: Implications for EGS Development. Proceedings, 30th Workshop on Geothermal Reservoir Engineering.

Link, P. K., 2002. Cassia County, ID, geologic map, Digital Atlas of Idaho, Idaho State University, Geosciences Department.

Mabey, D.R., Hoover, D.B, O'Donnell, J.E. and Wilson C. W., 1978, Reconnaissance geophysical studies of the geothermal systems in southern Raft River valley, Idaho: Geophysics, 43, 1470-1484.

Masi, U., O'Neil, J.R., and Kistler, R.W. (1981), "Stable isotope systematics in Mesozoic granites of central and northern California and southwestern Oregon," Contributions to Mineralogy and Petrology, 76, 116-126.

Moore, J.N, Allis, R.G., Nemčok, M., Powell, T.S., Bruton, C.J., Wannamaker, P.E., Raharjo, I.B., and Norman, D.I., 2008, The evolution of volcano-hosted geothermal systems based on deep wells from Karaha – Telaga Bodas, Indonesia: American Journal of Science, v. 308, p. 1-48.

Moore, J. N., Powell, T. S., Heizler, M. T., and Norman, D. I., 2000, Mineralization and hydrothermal history of the Tiwi geothermal system, Philippines: Economic Geology, v. 95, p. 1001-1023.

Nash, G.D., Moore, J.N., 2012, Raft River EGS project: a GIS-centric review of geology: GRC Transactions, v. 36, p. 951-958.

Newman, G.A., Gasperikova, E., Hoversten, G.M., Wannamaker, P.E., (2008). Three-dimensional magnetotelluric characterization of the Coso geothermal field. Geothermics. 37, 369-399.

O'Neil, J. R., 1986, *Theoretical and Experimental Aspects of Isotopic Fractionation,* in Stable Isotopes in High Temperature Geological Processes. J.W. Valley, H.P. Taylor, Jr. and J.R. O'Neil (eds), Reviews in Mineralogy 16, 1-37.

O'Neil, J.R., and Taylor, H.P. Jr. (1967), "The oxygen isotope and cation exchange chemistry of feldspars," J. Geophys. Res, 74**,** 6012-6022.

Rao, C. P. (1990), Petrography, trace elements and oxygen and carbon isotopes of Gordon Group carbonates (Ordovician), Florentine Valley, Tasmania, Australia. Sedimentary Geology, 66, 83-91.

Sheridan, J. Kovac, K., Rose, P.E., Barton, C., McCulloch J., Berard, B., Moore J.N., Petty, S., and Spielman, P. (2003), In situ stress, fracture and fluid flow analysis- East Flank of the Coso Geothermal field. Proceedings 28th Workshop of Geothermal Reservoir Engineering.

Simpson, F., and K. Bahr, 2005, Practical Magnetotellurics: University Press, Cambridge, 270 pp.

Siripunvaraporn, W., G. Egbert, Y. Lenbury, and M. Uyeshima, 2005, Three-dimensional magnetotelluric inversion: data-space method: Phys. Earth Planet. Inter., 150, 3-14.

Spichak, V., and Manzella, A., 2009, Electromagnetic sounding of geothermal zones: Journal of Applied Geophysics, v. 68, p. 459–478, doi: 10.1016/j.jappgeo.2008.05.007.

Taylor, H.P., Jr., 1971, Oxygen isotope evidence for large-scale interaction between meteoric ground waters and Tertiary granodiorite intrusion, western Cascade Range, Oregon. J. Geophys. Res. 76, 7855-7874.

Uchida, T., and Sasaki, Y., 2006, Stable 3D inversion of MT data and its application to geothermal exploration: Exploration Geophysics, v. 37, p. 223–230.

USGS NR_GEO, 2005, A spatial database for the geology of the Northern Rocky Mountains - Idaho, Montana, and Washington, Edition: 1.0, Open-File Report 2005-1235, U.S. Geological Survey, Menlo Park, California.

Vozoff, K., 1991, The magnetotelluric method, *in* M. N. Nabighian, ed., Electromagnetic Methods In Applied Geophysics, Vol. 2, Chapter 8: Society of Exploration Geophysics, 641-711.

Wannamaker, P.E., Maris, V., and Hardwick, C.L., 2013, Basin and Rift Structure of the Central Black Rock Desert, Utah, and Initial Thermal Implications, From 3D Magnetotellurics: Geothermal Resources Council Transactions, v. 37, 41–44.

Wannamaker, P.E., Maris, V., Hasterok, D.P., and Doerner, W.M., 2011, Crustal scale resistivity structure, magmatic-hydrothermal connections, and thermal regionalization of the Great Basin, Geothermal Resources Council Transactions, v. 35, 1787–1790.

Wannamaker, P.E., Doerner, W.M., and Hasterok, D.P., 2007, Integrated Dense Array and Transect MT Surveying at Dixie Valley Geothermal Area, Nevada; Structural Controls, Hydrothermal Alteration and Deep Fluid Sources, *in* Proceedings, Thirty-Second Workshop on Geothermal Reservoir Engineering, Stanford University, 402–407.

Wannamaker, P.E., Caldwell, T.E., Doerner, and W.M., Jiracek, G.R. (2004). Fault zone fluids and seismicity in compressional and extensional environments inferred from electrical conductivity: the New Zealand Southern Alps and U.S. Great Basin. Earth Planet Space, 56, 1171-1176.

Wannamaker, P. E., and G. W. Hohmann, 1991, Electromagnetic induction studies, U. S. National Report to IUGG, Rev. Geophys., Supplement, 405-415.

Whitmarsh, R.S., 2002a, Geological map of the Cactus Peak 7.5˚ quadrangle, Inyo County, California, CD-ROM map, *in* Glazner, A.F., Walker, J.D., Bartley, J.M. eds., Geologic Evolution of the Mojave Desert and Southwestern Basin and Range: Geological Society of America Memoir 195.

Whitmarsh, R.S., 2002b, Geological map of the Petroglyph Canyon 7.5˚ quadrangle, Inyo County, California, CD-ROM map, *in* Glazner, A.F., Walker, J.D., Bartley, J.M. eds., Geologic Evolution of the Mojave Desert and Southwestern Basin and Range: Geological Society of America Memoir 195.

Williams, P.L., Pierce, K.L., McIntyre, D.H. and Schmidt, P.W., 1974, Preliminary geologic map of the southern Raft River valley, Cassia County, Idaho: U.S. Geological Survey Open File Report.